BABAR-CONF-07/003
SLAC-PUB-12668
arXiv:0707.2670 [hep-ex]
July 2007

Measurement of Moments of the Hadronic-Mass and -Energy Spectrum in Inclusive Semileptonic $\overline{B} \to X_c \ell^- \overline{\nu}$ Decays

B. Aubert,[1] M. Bona,[1] D. Boutigny,[1] Y. Karyotakis,[1] J. P. Lees,[1] V. Poireau,[1] X. Prudent,[1] V. Tisserand,[1] A. Zghiche,[1] J. Garra Tico,[2] E. Grauges,[2] L. Lopez,[3] A. Palano,[3] M. Pappagallo,[3] G. Eigen,[4] B. Stugu,[4] L. Sun,[4] G. S. Abrams,[5] M. Battaglia,[5] D. N. Brown,[5] J. Button-Shafer,[5] R. N. Cahn,[5] Y. Groysman,[5] R. G. Jacobsen,[5] J. A. Kadyk,[5] L. T. Kerth,[5] Yu. G. Kolomensky,[5] G. Kukartsev,[5] D. Lopes Pegna,[5] G. Lynch,[5] L. M. Mir,[5] T. J. Orimoto,[5] I. L. Osipenkov,[5] M. T. Ronan,[5,*] K. Tackmann,[5] T. Tanabe,[5] W. A. Wenzel,[5] P. del Amo Sanchez,[6] C. M. Hawkes,[6] A. T. Watson,[6] T. Held,[7] H. Koch,[7] M. Pelizaeus,[7] T. Schroeder,[7] M. Steinke,[7] D. Walker,[8] D. J. Asgeirsson,[9] T. Cuhadar-Donszelmann,[9] B. G. Fulsom,[9] C. Hearty,[9] T. S. Mattison,[9] J. A. McKenna,[9] A. Khan,[10] M. Saleem,[10] L. Teodorescu,[10] V. E. Blinov,[11] A. D. Bukin,[11] V. P. Druzhinin,[11] V. B. Golubev,[11] A. P. Onuchin,[11] S. I. Serednyakov,[11] Yu. I. Skovpen,[11] E. P. Solodov,[11] K. Yu. Todyshev,[11] M. Bondioli,[12] S. Curry,[12] I. Eschrich,[12] D. Kirkby,[12] A. J. Lankford,[12] P. Lund,[12] M. Mandelkern,[12] E. C. Martin,[12] D. P. Stoker,[12] S. Abachi,[13] C. Buchanan,[13] S. D. Foulkes,[14] J. W. Gary,[14] F. Liu,[14] O. Long,[14] B. C. Shen,[14] L. Zhang,[14] H. P. Paar,[15] S. Rahatlou,[15] V. Sharma,[15] J. W. Berryhill,[16] C. Campagnari,[16] A. Cunha,[16] B. Dahmes,[16] T. M. Hong,[16] D. Kovalskyi,[16] J. D. Richman,[16] T. W. Beck,[17] A. M. Eisner,[17] C. J. Flacco,[17] C. A. Heusch,[17] J. Kroseberg,[17] W. S. Lockman,[17] T. Schalk,[17] B. A. Schumm,[17] A. Seiden,[17] M. G. Wilson,[17] L. O. Winstrom,[17] E. Chen,[18] C. H. Cheng,[18] F. Fang,[18] D. G. Hitlin,[18] I. Narsky,[18] T. Piatenko,[18] F. C. Porter,[18] R. Andreassen,[19] G. Mancinelli,[19] B. T. Meadows,[19] K. Mishra,[19] M. D. Sokoloff,[19] F. Blanc,[20] P. C. Bloom,[20] S. Chen,[20] W. T. Ford,[20] J. F. Hirschauer,[20] A. Kreisel,[20] M. Nagel,[20] U. Nauenberg,[20] A. Olivas,[20] J. G. Smith,[20] K. A. Ulmer,[20] S. R. Wagner,[20] J. Zhang,[20] A. M. Gabareen,[21] A. Soffer,[21,†] W. H. Toki,[21] R. J. Wilson,[21] F. Winklmeier,[21] D. D. Altenburg,[22] E. Feltresi,[22] A. Hauke,[22] H. Jasper,[22] J. Merkel,[22] A. Petzold,[22] B. Spaan,[22] K. Wacker,[22] V. Klose,[23] M. J. Kobel,[23] H. M. Lacker,[23] W. F. Mader,[23] R. Nogowski,[23] J. Schubert,[23] K. R. Schubert,[23] R. Schwierz,[23] J. E. Sundermann,[23] A. Volk,[23] D. Bernard,[24] G. R. Bonneaud,[24] E. Latour,[24] V. Lombardo,[24] Ch. Thiebaux,[24] M. Verderi,[24] P. J. Clark,[25] W. Gradl,[25] F. Muheim,[25] S. Playfer,[25] A. I. Robertson,[25] J. E. Watson,[25] Y. Xie,[25] M. Andreotti,[26] D. Bettoni,[26] C. Bozzi,[26] R. Calabrese,[26] A. Cecchi,[26] G. Cibinetto,[26] P. Franchini,[26] E. Luppi,[26] M. Negrini,[26] A. Petrella,[26] L. Piemontese,[26] E. Prencipe,[26] V. Santoro,[26] F. Anulli,[27] R. Baldini-Ferroli,[27] A. Calcaterra,[27] R. de Sangro,[27] G. Finocchiaro,[27] S. Pacetti,[27] P. Patteri,[27] I. M. Peruzzi,[27,‡] M. Piccolo,[27] M. Rama,[27] A. Zallo,[27] A. Buzzo,[28] R. Contri,[28] M. Lo Vetere,[28] M. M. Macri,[28] M. R. Monge,[28] S. Passaggio,[28] C. Patrignani,[28] E. Robutti,[28] A. Santroni,[28] S. Tosi,[28] K. S. Chaisanguanthum,[29] M. Morii,[29] J. Wu,[29] R. S. Dubitzky,[30] J. Marks,[30] S. Schenk,[30] U. Uwer,[30] D. J. Bard,[31] P. D. Dauncey,[31] R. L. Flack,[31] J. A. Nash,[31] W. Panduro Vazquez,[31] M. Tibbetts,[31] P. K. Behera,[32] X. Chai,[32] M. J. Charles,[32] U. Mallik,[32] V. Ziegler,[32] J. Cochran,[33] H. B. Crawley,[33] L. Dong,[33] V. Eyges,[33] W. T. Meyer,[33] S. Prell,[33] E. I. Rosenberg,[33] A. E. Rubin,[33] Y. Y. Gao,[34] A. V. Gritsan,[34] Z. J. Guo,[34] C. K. Lae,[34] A. G. Denig,[35] M. Fritsch,[35] G. Schott,[35] N. Arnaud,[36] J. Béquilleux,[36] A. D'Orazio,[36] M. Davier,[36] G. Grosdidier,[36] A. Höcker,[36] V. Lepeltier,[36] F. Le Diberder,[36] A. M. Lutz,[36] S. Pruvot,[36] S. Rodier,[36] P. Roudeau,[36] M. H. Schune,[36] J. Serrano,[36] V. Sordini,[36] A. Stocchi,[36] W. F. Wang,[36] G. Wormser,[36] D. J. Lange,[37] D. M. Wright,[37] I. Bingham,[38] J. P. Burke,[38] C. A. Chavez,[38] I. J. Forster,[38] J. R. Fry,[38] E. Gabathuler,[38] R. Gamet,[38] D. E. Hutchcroft,[38] D. J. Payne,[38] K. C. Schofield,[38] C. Touramanis,[38] A. J. Bevan,[39] K. A. George,[39] F. Di Lodovico,[39] W. Menges,[39] R. Sacco,[39] G. Cowan,[40] H. U. Flaecher,[40] D. A. Hopkins,[40] S. Paramesvaran,[40] F. Salvatore,[40] A. C. Wren,[40] D. N. Brown,[41] C. L. Davis,[41] J. Allison,[42] N. R. Barlow,[42] R. J. Barlow,[42] Y. M. Chia,[42] C. L. Edgar,[42] G. D. Lafferty,[42] T. J. West,[42] J. I. Yi,[42] J. Anderson,[43] C. Chen,[43] A. Jawahery,[43] D. A. Roberts,[43] G. Simi,[43] J. M. Tuggle,[43] G. Blaylock,[44] C. Dallapiccola,[44] S. S. Hertzbach,[44] X. Li,[44] T. B. Moore,[44] E. Salvati,[44] S. Saremi,[44] R. Cowan,[45] D. Dujmic,[45] P. H. Fisher,[45] K. Koeneke,[45] G. Sciolla,[45] S. J. Sekula,[45] M. Spitznagel,[45] F. Taylor,[45] R. K. Yamamoto,[45] M. Zhao,[45] Y. Zheng,[45] S. E. Mclachlin,[46,*] P. M. Patel,[46] S. H. Robertson,[46] A. Lazzaro,[47] F. Palombo,[47] J. M. Bauer,[48] L. Cremaldi,[48] V. Eschenburg,[48] R. Godang,[48] R. Kroeger,[48] D. A. Sanders,[48] D. J. Summers,[48] H. W. Zhao,[48] S. Brunet,[49] D. Côté,[49] M. Simard,[49] P. Taras,[49] F. B. Viaud,[49] H. Nicholson,[50] G. De Nardo,[51] F. Fabozzi,[51,§] L. Lista,[51] D. Monorchio,[51] C. Sciacca,[51] M. A. Baak,[52] G. Raven,[52] H. L. Snoek,[52] C. P. Jessop,[53] K. J. Knoepfel,[53] J. M. LoSecco,[53] G. Benelli,[54] L. A. Corwin,[54] K. Honscheid,[54]

Contributed to International Europhysics Conference On High Energy Physics (EPS-HEP2007), 7/19/2007- 7/25/2007, Manchester, England, UK
Work supported in part by US Department of Energy contract DE-AC02-76SF00515
SLAC, Stanford University, Stanford, CA 94025

H. Kagan,[54] R. Kass,[54] J. P. Morris,[54] A. M. Rahimi,[54] J. J. Regensburger,[54] Q. K. Wong,[54] N. L. Blount,[55] J. Brau,[55] R. Frey,[55] O. Igonkina,[55] J. A. Kolb,[55] M. Lu,[55] R. Rahmat,[55] N. B. Sinev,[55] D. Strom,[55] J. Strube,[55] E. Torrence,[55] N. Gagliardi,[56] A. Gaz,[56] M. Margoni,[56] M. Morandin,[56] A. Pompili,[56] M. Posocco,[56] M. Rotondo,[56] F. Simonetto,[56] R. Stroili,[56] C. Voci,[56] E. Ben-Haim,[57] H. Briand,[57] G. Calderini,[57] J. Chauveau,[57] P. David,[57] L. Del Buono,[57] Ch. de la Vaissière,[57] O. Hamon,[57] Ph. Leruste,[57] J. Malclès,[57] J. Ocariz,[57] A. Perez,[57] J. Prendki,[57] L. Gladney,[58] M. Biasini,[59] R. Covarelli,[59] E. Manoni,[59] C. Angelini,[60] G. Batignani,[60] S. Bettarini,[60] M. Carpinelli,[60] R. Cenci,[60] A. Cervelli,[60] F. Forti,[60] M. A. Giorgi,[60] A. Lusiani,[60] G. Marchiori,[60] M. A. Mazur,[60] M. Morganti,[60] N. Neri,[60] E. Paoloni,[60] G. Rizzo,[60] J. J. Walsh,[60] M. Haire,[61] J. Biesiada,[62] P. Elmer,[62] Y. P. Lau,[62] C. Lu,[62] J. Olsen,[62] A. J. S. Smith,[62] A. V. Telnov,[62] E. Baracchini,[63] F. Bellini,[63] G. Cavoto,[63] D. del Re,[63] E. Di Marco,[63] R. Faccini,[63] F. Ferrarotto,[63] F. Ferroni,[63] M. Gaspero,[63] P. D. Jackson,[63] L. Li Gioi,[63] M. A. Mazzoni,[63] S. Morganti,[63] G. Piredda,[63] F. Polci,[63] F. Renga,[63] C. Voena,[63] M. Ebert,[64] T. Hartmann,[64] H. Schröder,[64] R. Waldi,[64] T. Adye,[65] G. Castelli,[65] B. Franek,[65] E. O. Olaiya,[65] S. Ricciardi,[65] W. Roethel,[65] F. F. Wilson,[65] S. Emery,[66] M. Escalier,[66] A. Gaidot,[66] S. F. Ganzhur,[66] G. Hamel de Monchenault,[66] W. Kozanecki,[66] G. Vasseur,[66] Ch. Yèche,[66] M. Zito,[66] X. R. Chen,[67] H. Liu,[67] W. Park,[67] M. V. Purohit,[67] J. R. Wilson,[67] M. T. Allen,[68] D. Aston,[68] R. Bartoldus,[68] P. Bechtle,[68] N. Berger,[68] R. Claus,[68] J. P. Coleman,[68] M. R. Convery,[68] J. C. Dingfelder,[68] J. Dorfan,[68] G. P. Dubois-Felsmann,[68] W. Dunwoodie,[68] R. C. Field,[68] T. Glanzman,[68] S. J. Gowdy,[68] M. T. Graham,[68] P. Grenier,[68] C. Hast,[68] T. Hryn'ova,[68] W. R. Innes,[68] J. Kaminski,[68] M. H. Kelsey,[68] H. Kim,[68] P. Kim,[68] M. L. Kocian,[68] D. W. G. S. Leith,[68] S. Li,[68] S. Luitz,[68] V. Luth,[68] H. L. Lynch,[68] D. B. MacFarlane,[68] H. Marsiske,[68] R. Messner,[68] D. R. Muller,[68] C. P. O'Grady,[68] I. Ofte,[68] A. Perazzo,[68] M. Perl,[68] T. Pulliam,[68] B. N. Ratcliff,[68] A. Roodman,[68] A. A. Salnikov,[68] R. H. Schindler,[68] J. Schwiening,[68] A. Snyder,[68] J. Stelzer,[68] D. Su,[68] M. K. Sullivan,[68] K. Suzuki,[68] S. K. Swain,[68] J. M. Thompson,[68] J. Va'vra,[68] N. van Bakel,[68] A. P. Wagner,[68] M. Weaver,[68] W. J. Wisniewski,[68] M. Wittgen,[68] D. H. Wright,[68] A. K. Yarritu,[68] K. Yi,[68] C. C. Young,[68] P. R. Burchat,[69] A. J. Edwards,[69] S. A. Majewski,[69] B. A. Petersen,[69] L. Wilden,[69] S. Ahmed,[70] M. S. Alam,[70] R. Bula,[70] J. A. Ernst,[70] V. Jain,[70] B. Pan,[70] M. A. Saeed,[70] F. R. Wappler,[70] S. B. Zain,[70] M. Krishnamurthy,[71] S. M. Spanier,[71] R. Eckmann,[72] J. L. Ritchie,[72] A. M. Ruland,[72] C. J. Schilling,[72] R. F. Schwitters,[72] J. M. Izen,[73] X. C. Lou,[73] S. Ye,[73] F. Bianchi,[74] F. Gallo,[74] D. Gamba,[74] M. Pelliccioni,[74] M. Bomben,[75] L. Bosisio,[75] C. Cartaro,[75] F. Cossutti,[75] G. Della Ricca,[75] L. Lanceri,[75] L. Vitale,[75] V. Azzolini,[76] N. Lopez-March,[76] F. Martinez-Vidal,[76,¶] D. A. Milanes,[76] A. Oyanguren,[76] J. Albert,[77] Sw. Banerjee,[77] B. Bhuyan,[77] K. Hamano,[77] R. Kowalewski,[77] I. M. Nugent,[77] J. M. Roney,[77] R. J. Sobie,[77] P. F. Harrison,[78] J. Ilic,[78] T. E. Latham,[78] G. B. Mohanty,[78] H. R. Band,[79] X. Chen,[79] S. Dasu,[79] K. T. Flood,[79] J. J. Hollar,[79] P. E. Kutter,[79] Y. Pan,[79] M. Pierini,[79] R. Prepost,[79] S. L. Wu,[79] and H. Neal[80]

(The *BABAR* Collaboration)

[1] *Laboratoire de Physique des Particules, IN2P3/CNRS et Université de Savoie, F-74941 Annecy-Le-Vieux, France*
[2] *Universitat de Barcelona, Facultat de Fisica, Departament ECM, E-08028 Barcelona, Spain*
[3] *Università di Bari, Dipartimento di Fisica and INFN, I-70126 Bari, Italy*
[4] *University of Bergen, Institute of Physics, N-5007 Bergen, Norway*
[5] *Lawrence Berkeley National Laboratory and University of California, Berkeley, California 94720, USA*
[6] *University of Birmingham, Birmingham, B15 2TT, United Kingdom*
[7] *Ruhr Universität Bochum, Institut für Experimentalphysik 1, D-44780 Bochum, Germany*
[8] *University of Bristol, Bristol BS8 1TL, United Kingdom*
[9] *University of British Columbia, Vancouver, British Columbia, Canada V6T 1Z1*
[10] *Brunel University, Uxbridge, Middlesex UB8 3PH, United Kingdom*
[11] *Budker Institute of Nuclear Physics, Novosibirsk 630090, Russia*
[12] *University of California at Irvine, Irvine, California 92697, USA*
[13] *University of California at Los Angeles, Los Angeles, California 90024, USA*
[14] *University of California at Riverside, Riverside, California 92521, USA*
[15] *University of California at San Diego, La Jolla, California 92093, USA*
[16] *University of California at Santa Barbara, Santa Barbara, California 93106, USA*
[17] *University of California at Santa Cruz, Institute for Particle Physics, Santa Cruz, California 95064, USA*
[18] *California Institute of Technology, Pasadena, California 91125, USA*
[19] *University of Cincinnati, Cincinnati, Ohio 45221, USA*
[20] *University of Colorado, Boulder, Colorado 80309, USA*
[21] *Colorado State University, Fort Collins, Colorado 80523, USA*
[22] *Universität Dortmund, Institut für Physik, D-44221 Dortmund, Germany*
[23] *Technische Universität Dresden, Institut für Kern- und Teilchenphysik, D-01062 Dresden, Germany*
[24] *Laboratoire Leprince-Ringuet, CNRS/IN2P3, Ecole Polytechnique, F-91128 Palaiseau, France*
[25] *University of Edinburgh, Edinburgh EH9 3JZ, United Kingdom*

[26]Università di Ferrara, Dipartimento di Fisica and INFN, I-44100 Ferrara, Italy
[27]Laboratori Nazionali di Frascati dell'INFN, I-00044 Frascati, Italy
[28]Università di Genova, Dipartimento di Fisica and INFN, I-16146 Genova, Italy
[29]Harvard University, Cambridge, Massachusetts 02138, USA
[30]Universität Heidelberg, Physikalisches Institut, Philosophenweg 12, D-69120 Heidelberg, Germany
[31]Imperial College London, London, SW7 2AZ, United Kingdom
[32]University of Iowa, Iowa City, Iowa 52242, USA
[33]Iowa State University, Ames, Iowa 50011-3160, USA
[34]Johns Hopkins University, Baltimore, Maryland 21218, USA
[35]Universität Karlsruhe, Institut für Experimentelle Kernphysik, D-76021 Karlsruhe, Germany
[36]Laboratoire de l'Accélérateur Linéaire, IN2P3/CNRS et Université Paris-Sud 11,
Centre Scientifique d'Orsay, B. P. 34, F-91898 ORSAY Cedex, France
[37]Lawrence Livermore National Laboratory, Livermore, California 94550, USA
[38]University of Liverpool, Liverpool L69 7ZE, United Kingdom
[39]Queen Mary, University of London, E1 4NS, United Kingdom
[40]University of London, Royal Holloway and Bedford New College, Egham, Surrey TW20 0EX, United Kingdom
[41]University of Louisville, Louisville, Kentucky 40292, USA
[42]University of Manchester, Manchester M13 9PL, United Kingdom
[43]University of Maryland, College Park, Maryland 20742, USA
[44]University of Massachusetts, Amherst, Massachusetts 01003, USA
[45]Massachusetts Institute of Technology, Laboratory for Nuclear Science, Cambridge, Massachusetts 02139, USA
[46]McGill University, Montréal, Québec, Canada H3A 2T8
[47]Università di Milano, Dipartimento di Fisica and INFN, I-20133 Milano, Italy
[48]University of Mississippi, University, Mississippi 38677, USA
[49]Université de Montréal, Physique des Particules, Montréal, Québec, Canada H3C 3J7
[50]Mount Holyoke College, South Hadley, Massachusetts 01075, USA
[51]Università di Napoli Federico II, Dipartimento di Scienze Fisiche and INFN, I-80126, Napoli, Italy
[52]NIKHEF, National Institute for Nuclear Physics and High Energy Physics, NL-1009 DB Amsterdam, The Netherlands
[53]University of Notre Dame, Notre Dame, Indiana 46556, USA
[54]Ohio State University, Columbus, Ohio 43210, USA
[55]University of Oregon, Eugene, Oregon 97403, USA
[56]Università di Padova, Dipartimento di Fisica and INFN, I-35131 Padova, Italy
[57]Laboratoire de Physique Nucléaire et de Hautes Energies,
IN2P3/CNRS, Université Pierre et Marie Curie-Paris6,
Université Denis Diderot-Paris7, F-75252 Paris, France
[58]University of Pennsylvania, Philadelphia, Pennsylvania 19104, USA
[59]Università di Perugia, Dipartimento di Fisica and INFN, I-06100 Perugia, Italy
[60]Università di Pisa, Dipartimento di Fisica, Scuola Normale Superiore and INFN, I-56127 Pisa, Italy
[61]Prairie View A&M University, Prairie View, Texas 77446, USA
[62]Princeton University, Princeton, New Jersey 08544, USA
[63]Università di Roma La Sapienza, Dipartimento di Fisica and INFN, I-00185 Roma, Italy
[64]Universität Rostock, D-18051 Rostock, Germany
[65]Rutherford Appleton Laboratory, Chilton, Didcot, Oxon, OX11 0QX, United Kingdom
[66]DSM/Dapnia, CEA/Saclay, F-91191 Gif-sur-Yvette, France
[67]University of South Carolina, Columbia, South Carolina 29208, USA
[68]Stanford Linear Accelerator Center, Stanford, California 94309, USA
[69]Stanford University, Stanford, California 94305-4060, USA
[70]State University of New York, Albany, New York 12222, USA
[71]University of Tennessee, Knoxville, Tennessee 37996, USA
[72]University of Texas at Austin, Austin, Texas 78712, USA
[73]University of Texas at Dallas, Richardson, Texas 75083, USA
[74]Università di Torino, Dipartimento di Fisica Sperimentale and INFN, I-10125 Torino, Italy
[75]Università di Trieste, Dipartimento di Fisica and INFN, I-34127 Trieste, Italy
[76]IFIC, Universitat de Valencia-CSIC, E-46071 Valencia, Spain
[77]University of Victoria, Victoria, British Columbia, Canada V8W 3P6
[78]Department of Physics, University of Warwick, Coventry CV4 7AL, United Kingdom
[79]University of Wisconsin, Madison, Wisconsin 53706, USA
[80]Yale University, New Haven, Connecticut 06511, USA

(Dated: July 18, 2007)

We present a measurement of moments of the inclusive hadronic-mass and -energy spectrum in semileptonic $\overline{B} \to X_c \ell^- \overline{\nu}$ decays. This study is based on a sample of 232 million $\Upsilon(4S) \to B\overline{B}$ decays recorded by the *BABAR* detector at the PEP-II e^+e^--storage rings. We reconstruct the semileptonic decay by identifying a lepton in events tagged by a fully reconstructed hadronic decay of the second B meson. We report preliminary results for the moments $\langle m_X^k \rangle$ with $k = 1, \ldots, 6$ and $\langle n_X^k \rangle$ with $k = 2, 4, 6$ and $n_X^2 = m_X^2 c^4 - 2\tilde{\Lambda} E_X + \tilde{\Lambda}^2$, with m_X the mass of the hadronic system, E_X its energy, and $\tilde{\Lambda}$ a constant of 0.65 GeV, for different minimal lepton momenta between 0.8 and 1.9 GeV/c measured in the B-meson rest frame. These are predicted in the framework of a Heavy Quark Expansion (HQE), which allows the extraction of the total semileptonic branching fraction, the CKM-matrix element $|V_{cb}|$, and the quark masses m_b and m_c, together with the dominant non-perturbative HQE parameters. We find as preliminary results $|V_{cb}| = (41.88 \pm 0.81) \cdot 10^{-3}$ and $m_b = (4.552 \pm 0.055)\,\mathrm{GeV}/c^2$.

Submitted to the 2007 Europhysics Conference on High Energy Physics, Manchester, England.

PACS numbers: 12.15.Ff, 12.15.Hh, 13.25.Hw, 13.30.Ce

I. INTRODUCTION

Measurement of moments of the hadronic-mass [1–5] and lepton-energy [4, 6, 7] spectra in inclusive semileptonic decays $\overline{B} \to X_c \ell^- \overline{\nu}$ have been used to determine the non-perturbative QCD parameters describing these decays and the CKM matrix element $|V_{cb}|$.

Combined fits to these moments and moments of the photon-energy spectrum in $B \to X_s \gamma$ decays [8–11] in the context of Heavy Quark Expansions (HQE) of QCD have resulted in precise determinations of $|V_{cb}|$ and m_b, the mass of the b quark. Specifically, they are reported to be $|V_{cb}| = (42.0 \pm 0.2 \pm 0.7) \cdot 10^{-3}$ and $m_b = (4.59 \pm 0.03 \pm 0.03)\,\mathrm{GeV}/c^2$ in the kinetic mass scheme [12] and $|V_{cb}| = (41.4 \pm 0.6 \pm 0.1) \cdot 10^{-3}$ and $m_b = (4.68 \pm 0.03)\,\mathrm{GeV}/c^2$ in the 1S scheme [13].

Lepton-energy moments are known with very good accuracy, but the precision of the hadronic-mass and photon-energy moments is limited by statistics. Therefore, we present here an updated measurement of the hadronic-mass moments $\langle m_X^k \rangle$ with $k = 1, \ldots, 6$ based on a larger dataset than previously used [2]. In addition we present measurements of the mixed hadron mass-energy moments $\langle n_X^k \rangle$ with $k = 2, 4, 6$ as proposed by Gambino and Uraltsev [14]. All moments are presented for different cuts on the minimum energy of the charged lepton. The mixed moments use the mass m_X and the energy E_X of the X_c system in the B meson rest frame of $\overline{B} \to X_c \ell^- \overline{\nu}$ decays,

$$n_X^2 = m_X^2 c^4 - 2\tilde{\Lambda} E_X + \tilde{\Lambda}^2, \tag{1}$$

with a constant $\tilde{\Lambda}$, here fixed to be 0.65 GeV as proposed in [14]. They allow a more reliable extraction of the higher-order non-perturbative HQE parameters and thus they are expected to increase the precision on the extraction of $|V_{cb}|$ and the quark masses m_b and m_c.

We perform a combined fit to the hadronic mass moments, measured moments of the lepton-energy spectrum, and moments of the photon energy spectrum in decays $B \to X_s \gamma$. The fit extracts values for $|V_{cb}|$, the quark masses m_b and m_c, the total semileptonic branching fraction $\mathcal{B}(\overline{B} \to X_c \ell^- \overline{\nu})$, and the dominant non-perturbative HQE parameters. These are μ_π^2 and μ_G^2, parameterizing effects at $\mathcal{O}(1/m_b^2)$, and ρ_D^3 and ρ_{LS}^3, parameterizing effects at $\mathcal{O}(1/m_b^3)$.

II. *BABAR* DETECTOR AND DATASET

The analysis is based on data collected with the *BABAR* experiment [15] at the PEP-II asymmetric-energy e^+e^- storage rings [16] at the Stanford Linear Accelerator Center between October 1999 and July 2004.

The *BABAR* tracking system used for charged particle and vertex reconstruction has two main components: a silicon vertex tracker (SVT) and a drift chamber (DCH), both operating within a 1.5-T magnetic field of a superconducting solenoid. The transverse momentum resolution is 0.47 % at 1 GeV/c. Photons are identified in an electromagnetic calorimeter (EMC) surrounding a detector of internally reflected Cherenkov light (DIRC), which associates Cherenkov photons with tracks for particle identification (PID). The energy of photons is measured with a resolution of 3 % at 1 GeV. Muon candidates are identified with the use of the instrumented flux return (IFR) of the solenoid. The detector covers the polar angle of $30^\circ < \theta < 140^\circ$ in the center of mass (c.m.) frame.

The data sample consists of about 210.4 fb^{-1}, corresponding to $(232 \pm 3) \times 10^6$ decays of $\Upsilon(4S) \to B\overline{B}$. We use Monte Carlo (MC) simulated events to determine background distributions and to correct for detector acceptance and resolution effects. The simulation of the *BABAR* detector is realized with `GEANT4` [17]. Simulated B meson decays are generated using `EvtGen` [18]. Final state radiation is modeled with `PHOTOS` [19].

The simulations of $\overline{B} \to X_c \ell^- \overline{\nu}$ decays use a parameterization of form factors for $\overline{B} \to D^* \ell^- \overline{\nu}$ [20], and models for $\overline{B} \to D \ell^- \overline{\nu}, D^{**} \ell^- \overline{\nu}$ [21] and $\overline{B} \to D\pi \ell^- \overline{\nu}, D^* \pi \ell^- \overline{\nu}$ [22].

*Deceased
†Now at Tel Aviv University, Tel Aviv, 69978, Israel
‡Also with Università di Perugia, Dipartimento di Fisica, Perugia, Italy
§Also with Università della Basilicata, Potenza, Italy
¶Also with Universitat de Barcelona, Facultat de Fisica, Departament ECM, E-08028 Barcelona, Spain

III. RECONSTRUCTION OF SEMILEPTONIC DECAYS

A. Selection of Hadronic B-Meson Decays

The analysis uses $\Upsilon(4S) \to B\overline{B}$ events in which one of the B mesons decays to hadrons and is fully reconstructed ($B_{\rm reco}$) and the semileptonic decay of the recoiling $\overline{B}$ meson ($B_{\rm recoil}$) is identified by the presence of an electron or muon. While this approach results in a low overall event selection efficiency of only a few per mille, it allows for the determination of the momentum, charge, and flavor of the B mesons. To obtain a large sample of B mesons, many exclusive hadronic decays are reconstructed [23]. The kinematic consistency of these $B_{\rm reco}$ candidates is checked with two variables, the beam-energy-substituted mass $m_{\rm ES} = \sqrt{s/4 - \vec{p}_B^{\,2}}$ and the energy difference $\Delta E = E_B - \sqrt{s}/2$. Here $\sqrt{s}$ is the total energy in the c.m. frame, $\vec{p}_B$ and E_B denote the c.m. momentum and c.m. energy of the $B_{\rm reco}$ candidate. We require $\Delta E = 0$ within three standard deviations, which range between 10 and 30 MeV depending on the number of hadrons used for the reconstruction. For a given $B_{\rm reco}$ decay mode, the purity is estimated as the signal fraction in events with $m_{\rm ES} > 5.27\,{\rm GeV}/c^2$. For events with one high-momentum lepton with $p^*_\ell \geq 0.8\,{\rm GeV}/c$ in the B-meson rest frame, the purity is approximately 78 %.

B. Selection of Semileptonic Decays

Semileptonic decays are identified by the presence of one and only one electron or muon above a minimum momentum $p^*_{\ell,\rm min}$ measured in the rest frame of the $B_{\rm recoil}$. Electrons are selected with 94% average efficiency and a hadron misidentification rate in the order of 0.1%. Muons are identified with an efficiency ranging between 60% for momenta $p = 1\,{\rm GeV}/c$ in the laboratory frame and 75% for momenta $p > 2\,{\rm GeV}/c$ and a hadron misidentification rate between 1% for kaons and protons and 3% for pions. Efficiencies and misidentification rates are estimated from selected samples of electrons, muons, pions, and kaons. We impose the condition $Q_b Q_\ell < 0$, where Q_ℓ is the charge of the lepton and Q_b is the charge of the b-quark of the $B_{\rm reco}$. This condition is fulfilled for primary leptons, except for $B^0\overline{B}^0$ events in which flavor mixing has occurred. We require the total observed charge of the event to be $|Q_{\rm tot}| = |Q_{\rm B_{reco}} + Q_{\rm B_{recoil}}| \leq 1$, allowing for a charge imbalance in events with low momentum tracks or photon conversions. In cases where only one charged track is present in the reconstructed X_c system, the total charge in the event is required to be equal to zero.

C. Reconstruction of the Hadronic System

The hadronic system X_c in the decay $\overline{B} \to X_c \ell^- \overline{\nu}$ is reconstructed from charged tracks and energy depositions in the calorimeter that are not associated with the $B_{\rm reco}$ or the charged lepton. Procedures are implemented to eliminate fake tracks, low-energy beam-generated photons, and energy depositions in the calorimeter originating from hadronic showers faking the presence of additional particles. Each track is assigned a specific particle type, either $\overset{(-)}{p}$, $K^\pm$, or $\pi^\pm$, based on combined information from the different *BABAR* subdetectors. The four-momentum of the reconstructed hadronic system P_{X_c} is calculated from the four-momenta of the reconstructed tracks $P_{i,trk}$, reconstructed using the mass of the identified particle type, and photons $P_{i,\gamma}$ by $P_{X_c} = \sum_{i=1}^{N_{trk}} P_{i,trk} + \sum_{i=1}^{N_\gamma} P_{i,\gamma}$. The hadronic mass m_X is calculated from the reconstructed four-momenta as $m_X = \sqrt{P^2_{X_c}}$.

The four-momentum of the unmeasured neutrino P_ν is estimated from the missing four-momentum $P_{\rm miss} = P_{\Upsilon(4S)} - P_{B_{\rm reco}} - P_{X_c} - P_\ell$. Here, all four-momenta are measured in the laboratory frame. To ensure a well reconstructed hadronic system, we impose criteria on the missing energy, $E_{\rm miss} > 0.5\,{\rm GeV}$, the missing momentum, $|\vec{p}_{\rm miss}| > 0.5\,{\rm GeV}/c$, and the difference of both quantities, $|E_{\rm miss} - c|\vec{p}_{\rm miss}|| < 0.5\,{\rm GeV}$. After having selected a well reconstructed $B_{\rm reco}$ and having imposed the selection criteria on $E_{\rm miss} - c|\vec{p}_{\rm miss}|$, 4.7% of signal decays and 0.3% of background decays are retained.

Starting from a kinematically well defined initial state additional knowledge of the kinematics of the semileptonic final state is used in a kinematic fit to improve the overall resolution and reduce the bias of the measured values. The fit imposes four-momentum conservation, the equality of the masses of the two B mesons, and constrains the mass of the neutrino, $P^2_\nu = 0$. The resulting average resolutions in m_X and n^2_X are $0.355\,{\rm GeV}/c^2$ and $1.31\,{\rm GeV}^2$, respectively. The overall biases of the kinematically fitted hadronic system are found to be $-0.096\,{\rm GeV}/c^2$ and $-0.08\,{\rm GeV}^2$, respectively. We require the fit to converge, thus ensuring that the constraints are fulfilled.

The background is composed of $e^+e^- \to q\overline{q}\,(q = u, d, s, c)$ events (continuum background) and decays $\Upsilon(4S) \to B^+B^-$ or $B^0\overline{B}^0$ in which the $B_{\rm reco}$ candidate is mistakenly reconstructed from particles coming from both B mesons in the event (combinatorial background). Missing tracks and photons in the reconstructed hadronic system are not considered an additional source of background since they only affect its resolution. The effect of missing particles in the reconstruction is taken care of by further correction procedures. To quantify the amount of background in the $m_{\rm ES}$ signal region we perform a fit to the $m_{\rm ES}$ distribution of the $B_{\rm reco}$ candidates. We parametrize the background using an empirical threshold

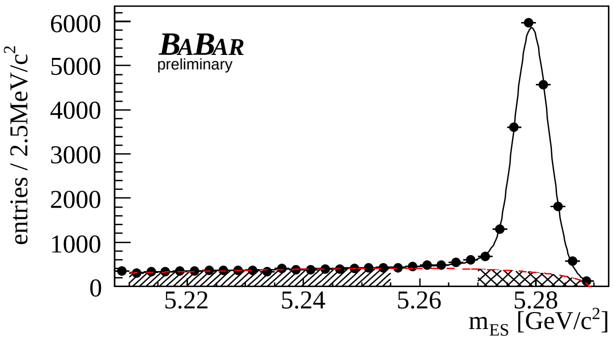

FIG. 1: $m_{\rm ES}$ spectrum of $B_{\rm reco}$ decays accompanied by a lepton with $p^*_\ell \geq 0.8\,{\rm GeV}/c$. The signal (solid line) and background (red dashed line) components of the fit are overlaid. The crossed area shows the background under the $B_{\rm reco}$ signal. The background control region in the $m_{\rm ES}$ sideband is indicated by the hatched area.

function [24],

$$\frac{{\rm d}N}{{\rm d}m_{\rm ES}} \propto m_{\rm ES}\sqrt{1-x^2}e^{-\chi\left(1-x^2\right)}, \qquad (2)$$

where $x = m_{\rm ES}/m_{\rm ES,max}$, $m_{\rm ES,max} = 5.289\,{\rm GeV}/c^2$ is the kinematic endpoint approximated by the mean c.m. energy, and χ is a free parameter defining the curvature of the function. The signal is parameterized with a modified Gaussian function [25] peaked at the B-meson mass and corrected for radiation losses. The fit is performed separately for several bins in m_X and n_X^2 to account for changing background contributions in different m_X or n_X^2 regions, respectively. The background shape is determined in a signal-free region of the $m_{\rm ES}$ sideband, $5.21 \leq m_{\rm ES} \leq 5.255\,{\rm GeV}/c^2$. Figure 1 shows the $m_{\rm ES}$ distribution for $p^*_\ell \geq 0.8\,{\rm GeV}/c$ together with the fitted signal and background contributions.

Residual background is estimated from MC simulations. It is composed of charmless semileptonic decays $\overline{B} \to X_u\ell^-\overline{\nu}$, hadrons misidentified as leptons, secondary leptons from semileptonic decays of $D^{(*)}$, D_s^+ mesons or τ either in $B^0\overline{B}^0$ mixed events or produced in $b \to c\overline{c}s$ transitions, as well as leptons from decays of J/ψ, and $\psi(2S)$. The simulated background spectra are normalized to the number of $B_{\rm reco}$ events in data. We verify the normalization using an independent data control sample with inverted lepton charge correlation, $Q_bQ_\ell > 0$.

IV. HADRONIC MASS MOMENTS

We present measurements of the moments $\langle m_X^k\rangle$, with $k = 1, \ldots 6$, of the hadronic mass distribution in semileptonic B meson decays $\overline{B} \to X_c\ell^-\overline{\nu}$. The moments are measured as functions of the lower limit on the lepton momentum, $p^*_{\ell,{\rm min}}$, between $0.8\,{\rm GeV}/c$ and $1.9\,{\rm GeV}/c$ calculated in the rest frame of the B meson.

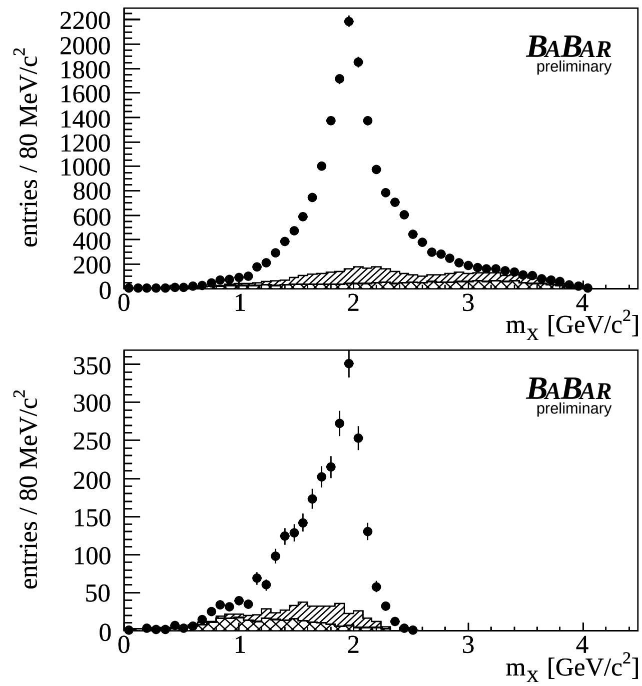

FIG. 2: Kinematically fitted hadronic mass spectra for minimal lepton momenta $p^*_\ell \geq 0.8\,{\rm GeV}/c$ (top) and $p^*_\ell \geq 1.9\,{\rm GeV}/c$ (bottom) together with distributions of combinatorial background and background from non-$B\overline{B}$ decays (hatched area) as well as residual background (crossed area)

A. Selected Event Sample

The selected event sample contains about 21.5% background. For $p^*_\ell \geq 0.8\,{\rm GeV}/c$ we find a total of 15085 ± 146 signal events above a combinatorial and continuum background of 2429 ± 43 events and residual background of 1696 ± 19 events. For $p^*_\ell \geq 1.9\,{\rm GeV}/c$ we find 2006 ± 53 signal events above a background constituted of 271 ± 17 and 248 ± 7 combinatorial and residual events, respectively. Figure 2 shows the kinematically fitted m_X distributions together with the extracted background shapes for $p^*_\ell \geq 0.8\,{\rm GeV}/c$ and $p^*_\ell \geq 1.9\,{\rm GeV}/c$.

B. Extraction of Moments

To extract unbiased moments $\langle m_X^k\rangle$, additional corrections have to be applied to correct for remaining effects that can distort the measured m_X distribution. Contributing effects are the limited acceptance and resolution of the *BABAR* detector resulting in unmeasured particles and in misreconstructed energies and momenta of particles. Additionally measured particles not originating from the hadronic system and final state radiation of leptons contribute, too. We correct the kinematically fitted m_X^k by applying correction factors on an event-by-event basis using the observed linear relationship between the moments of the measured mass $\langle m^k_{X,reco}\rangle$ and moments of the true underlying mass $\langle m^k_{X,true}\rangle$. Correction functions are constructed from MC simulations by calculating moments $\langle m^k_{X,reco}\rangle$ and $\langle m^k_{X,true}\rangle$ in several bins of the true mass $m_{X,true}$ and fitting the observed dependence with a linear function.

Studies show that the bias of the measured $\langle m^k_{X,reco}\rangle$ is not constant over the whole phase space but depends on the resolution and total multiplicity of the reconstructed hadronic system, N_{X_c}. Therefore, correction functions are derived in three bins of N_{X_c}, three bins of $E_{\rm miss}-c|\vec{p}_{\rm miss}|$, as well as in twelve bins of p^*_ℓ, each with a width of 100 MeV/c. Due to limited number of generated MC events, the binning in N_{X_c} and $E_{\rm miss}-c|\vec{p}_{\rm miss}|$ is abandoned for $p^*_{\ell,\rm min}\geq 1.7\,{\rm GeV}/c$. Overall we construct 75 calibration functions for each order of moments. Figure 3 shows examples of correction functions for the moment $\langle m^2_X\rangle$ in three bins of p^*_ℓ as well as in nine bins of $E_{\rm miss}-c|\vec{p}_{\rm miss}|$ and N_{X_c}.

For each event i the corrected mass $m^k_{X,calib,i}$ is calculated by inverting the linear function,

$$m^k_{X,calib,i}=\frac{m^k_{X,reco,i}-A(E_{\rm miss}-c|\vec{p}_{\rm miss}|,N_{X_c},k,p^*_\ell)}{B(E_{\rm miss}-c|\vec{p}_{\rm miss}|,N_{X_c},k,p^*_\ell)}, \quad (3)$$

with A the offset and B the slope of the correction function. Background contributions are subtracted by applying weight factors w_i dependent on $m_{X,reco}$ to each corrected hadronic mass, whereby each weight corresponds to the fraction of signal events expected in the corresponding part of the $m_{X,reco}$ spectrum. This leads to the following expression used for the calculation of the moments:

$$\langle m^k_X\rangle=\frac{\sum\limits_{i=1}^{N_{ev}} w_i\, m^k_{X,calib,i}}{\sum\limits_{i}^{N_{ev}} w_i}\times\mathcal{C}_{calib}\times\mathcal{C}_{true}. \quad (4)$$

The factors $\mathcal{C}_{calib}$ and $\mathcal{C}_{true}$ are dependent on the order k and minimal lepton momentum $p^*_{\ell,\rm min}$ of the measured moment. They are determined in MC simulations and correct for small biases observed after the calibration. The factors $\mathcal{C}_{calib}$ account for the bias of the applied correction method and range between 0.985 and 0.996. For $\langle m^6_X\rangle$ we observe larger biases ranging between 0.897 and 0.970 for the lowest $p^*_{\ell,\rm min}$ between 0.8 GeV/c and 1.2 GeV/c, respectively. The residual bias correction factor $\mathcal{C}_{true}$ accounts for differences in selection efficiencies for different hadronic final states and QED radiation in the final state that is included in the measured hadron mass and distorts the measurement of the lepton's momentum. The effect of radiative photons is estimated by employing PHOTOS. Our correction procedure results in moments which are free of photon radiation. The residual bias correction $\mathcal{C}_{true}$ is estimated in MC simulations and typically ranges between 0.994 and 1.014. For the moments $\langle m^5_X\rangle$ and $\langle m^6_X\rangle$ slighly higher correction factors are determined ranging between 0.994 and 1.023 as well as 0.994 and 1.036, respectively.

This procedure is verified on a MC sample by applying the calibration to measured hadron masses of individual semileptonic decays, $\overline{B}\to D\ell^-\nu$, $\overline{B}\to D^*\ell^-\nu$, four resonant decays $B\to D^{**}\ell\nu$, and two non-resonant decays $B\to D^{(*)}\pi\ell\nu$. Figure 4 shows the corrected moments $\langle m^2_X\rangle$ and $\langle m^4_X\rangle$ as functions of the true moments for minimal lepton momenta $p^*_\ell\geq 0.8\,{\rm GeV}/c$. The dashed line corresponds to $\langle m^k_{X,calib}\rangle=\langle m^k_{X,true}\rangle$. The calibration reproduces the true moments over the full mass range.

C. Systematic Studies

The principal systematic uncertainties are associated with the modeling of hadronic final states in semileptonic B-meson decays, the bias of the calibration method, the subtraction of residual background contributions, the modeling of track and photon selection efficiencies, the identification of particles, as well as the stability of the results. The obtained results are summarized in Tables A.I and A.II for the measured moments $\langle m^k_X\rangle$ with $k=1\ldots 6$ and selection criteria on the minimum lepton momentum ranging from $p^*_\ell\geq 0.8\,{\rm GeV}/c$ to $p^*_\ell\geq 1.9\,{\rm GeV}/c$.

1. *Modeling of Signal Decays*

The uncertainty of the calibration method with respect to the chosen signal model is estimated by changing the composition of the simulated inclusive hadronic spectrum. The dependence on the simulation of high mass hadronic final states is estimated by constructing correction functions only from MC simulated hadronic events with hadronic masses $m_{X,true,cut}<2.5\,{\rm GeV}/c^2$, thereby removing the high mass tail of the simulated hadronic mass spectrum. The model dependence of the calibration method is found to contribute only little to the total systematic uncertainty. We estimate the model dependence of the residual bias correction $\mathcal{C}_{true}$ by changing the composition of the inclusive hadronic spectrum, thereby omitting one or more decay modes. We associate a systematic uncertainty to the correction of the observed bias of the calibration method $\mathcal{C}_{calib}$ of half the size of the applied correction.

We study the effect of differences between data and MC in the multiplicity and $E_{\rm miss}-c|\vec{p}_{\rm miss}|$ distributions on the calibration method by changing the binning of the correction functions. The observed variation of the results is found to be covered by the statistical uncertainties of the calibration functions.

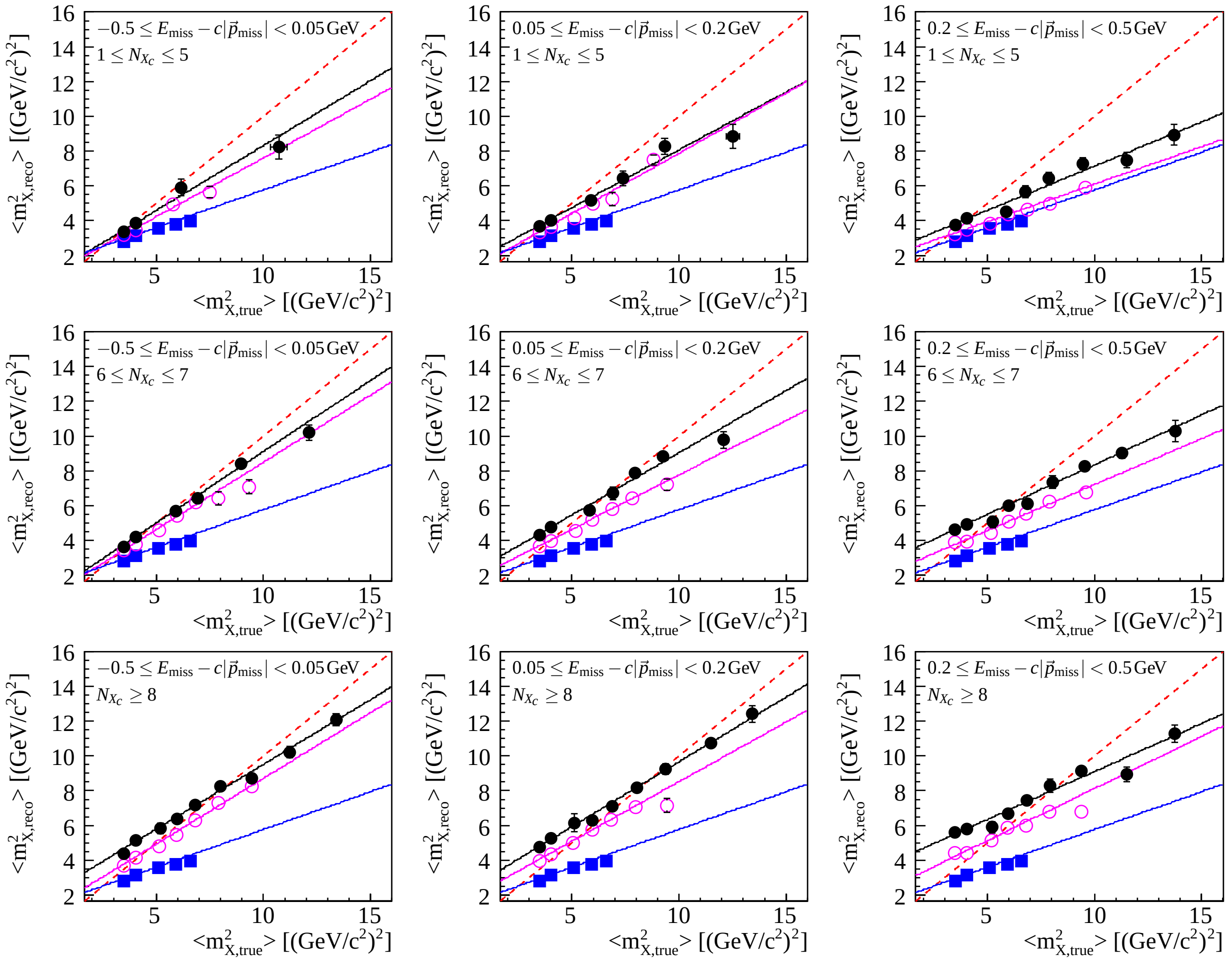

FIG. 3: Examples of calibration fucntions for $\langle m_X^2\rangle$ in bins of N_{X_c}, $E_{\rm miss} - c|\vec{p}_{\rm miss}|$ and p^*_ℓ. Shown are the extracted $\langle m_{X,reco}\rangle$ versus $\langle m_{X,true}\rangle$ in bins of $m_{X,true}$ for $0.8 \le p^*_\ell < 0.9\,$GeV/c (●), $1.4 \le p^*_\ell < 1.5\,$GeV/c (○), and $p^*_\ell \ge 1.9\,$GeV/c (■). The results of fits of linear functions are overlaid as solid lines. A reference line with $\langle m_{X,reco}\rangle = \langle m_{X,true}\rangle$ is superimposed (dashed line). There is only one calibration function with $p^*_\ell \ge 1.9\,$GeV/c constructed but plotted for better comparableness in each bin.

2. *Background Subtraction*

The branching fractions of background decays in the MC simulation are scaled to agree with current measurements [26]. The associated systematic uncertainty is estimated by varying these branching fractions within their uncertainties. At low $p^*_{\ell,\rm min}$, most of the studied background channels contribute to the systematic uncertainty, while at high $p^*_{\ell,\rm min}$, the systematic uncertainty is dominated by background from decays $\overline{B} \to X_u \ell^- \overline{\nu}$. Contributions from J/ψ and $\psi(2S)$ decays are found to be negligible.

The uncertainty in the combinatorial $B_{\rm reco}$ background subtraction is estimated by varying the lower and upper limits of the sideband region in the $m_{\rm ES}$ distribution up and down by $2.5\,{\rm MeV}/c^2$. The observed effect is found to be negligible.

3. *Detector-Related Effects*

We correct the MC simulation for differences to data in the selection efficiencies of charged tracks and photons, as well as identification efficiencies and misidentification rates of various particle types. The corrections are extracted from data and MC control samples.

The uncertainty of the photon selection efficiencies is found to be 1.8% per photon independent of energy, polar angle and multiplicity. The systematic uncertainty in track finding efficiencies is estimated to be 0.8% per track. We add in quadrature the statistical uncertainty of the control samples that depend on energy and polar angle of the track as well as the multiplicity of tracks in the reconstructed event. The misidentification of $\pi^\pm$ mesons as leptons is found to affect the overall normalization of the corresponding background spectra by 8%.

While the latter two uncertainties give only small contributions to the total systematic uncertainty, the uncer-

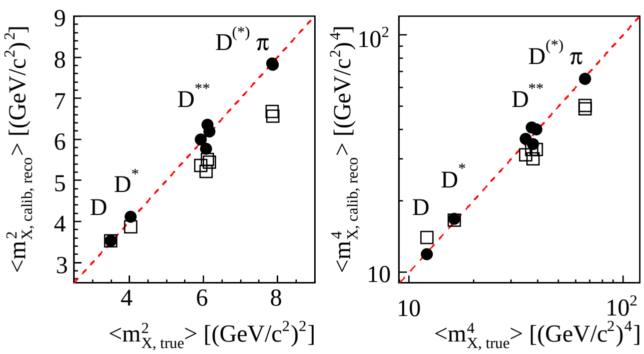

FIG. 4: Calibrated (•) and uncorrected (□) moments $\langle m_X^2\rangle$ (left) and $\langle m_X^4\rangle$ (right) of individual hadronic modes for minimal lepton momenta $p_\ell^* \geq 0.8\,\mathrm{GeV}/c$. A reference line with $\langle m_{X,calib}\rangle = \langle m_{X,true}\rangle$ is superimposed.

tainty associated with the selection efficiency of photons is found to be the main source of systematic uncertainties.

4. Stability of the Results

The stability of the results is tested by dividing the data into several independent subsamples: $B^\pm$ and B^0, decays to electrons and muons, different run periods of roughly equal data-sample sizes, and two regions in the $E_{\rm miss}-c|\vec{p}_{\rm miss}|$ spectrum, $-0.5 \leq E_{\rm miss}-c|\vec{p}_{\rm miss}| < 0\,\mathrm{GeV}$ and $0 \leq E_{\rm miss}-c|\vec{p}_{\rm miss}| < 0.5\,\mathrm{GeV}$, characterized by different resolutions of the reconstructed hadronic system. No significant variations are observed.

The stability of the result under variation of the selection criteria on $E_{\rm miss}-c|\vec{p}_{\rm miss}|$ is tested by varying the applied cut between $|E_{\rm miss}-c|\vec{p}_{\rm miss}|| < 0.2\,\mathrm{GeV}$ and $|E_{\rm miss}-c|\vec{p}_{\rm miss}|| < 1.4\,\mathrm{GeV}$. For most of the measured moments the observed variation is covered by other known systematic detector and MC simulation effects. In cases where the observed variation is not covered by those effects, we add an additional contribution to the systematic uncertainty of the measurement that compensates the observed difference .

5. Simulation of Radiation

We check the impact of low energetic photons by removing EMC neutral energy deposits with energies below 100 MeV from the reconstructed hadronic system. The effect on the measured moments is found to be negligible.

D. Results

The measured hadronic mass moments $\langle m_X^k\rangle$ with $k = 1\ldots6$ as functions of the minimal lepton momentum $p^*_{\ell,\rm min}$ are depicted in Fig. 5. All measurements are correlated since they share subsets of selected events. Tables A.I and A.II summarize the numerical results. The statistical uncertainty consists of contributions from the data statistics and the statistics of the MC simulation used for the construction of the correction functions, for the subtraction of residual background, and the determination of the final bias correction. In most cases we find systematic uncertainties that exceed the statistical uncertainty by a factor of 1.5.

V. MIXED HADRONIC MASS- AND ENERGY-MOMENTS

The measurement of moments of the observable n_X^2, a combination of the mass and energy of the inclusive X_c system, as defined in Eq. 1 , allow a more reliable extraction of the higher order HQE parameters μ_π^2, μ_G^2, ρ_D^3, and ρ_{LS}^3. Thus a smaller uncertainty on the standard model parameters $|V_{cb}|$, m_b, and m_c could be achieved.

We present measurements of the moments $\langle n_X^2\rangle$, $\langle n_X^4\rangle$, and $\langle n_X^6\rangle$ for different minimal lepton momenta between 0.8 GeV/c and 1.9 GeV/c calculated in the B-meson rest frame. We calculate the central moments $\langle(n_X^2-\langle n_X^2\rangle)^2\rangle$, $\langle(n_X^2-\langle n_X^2\rangle)^3\rangle$, and the moments $\langle(n_X^2-1.35\ \mathrm{GeV}^2)^2\rangle$ and $\langle(n_X^2-1.35\ \mathrm{GeV}^2)^3\rangle$ as proposed in [14].

Due to the structure of the variable n_X^2 as a difference of two measured values, its measured resolution and bias are larger than for the mass moments and the sensitivity to $E_{\rm miss}-c|\vec{p}_{\rm miss}|$ is increased wrt. to m_X. The overall resolution of n_X^2 after the kinematic fit for lepton momenta greater than 0.8 GeV/c is measured to be 1.31 GeV^2 with a bias of -0.08 GeV^2. We therefore introduce stronger requirements on the reconstruction quality of the event. We tighten the criteria on the neutrino observables. The variable $E_{\rm miss}-c|\vec{p}_{\rm miss}|$ is required to be between 0 and 0.3 GeV. Due to the stronger requirements on $E_{\rm miss}-c|\vec{p}_{\rm miss}|$ the individual variables $E_{\rm miss}$ and $|\vec{p}_{\rm miss}|$ have less influence on the resolution of the reconstrcuted hadronic system. Therefore, the cuts on the missing energy and the missing momentum in the event are loosened to $E_{\rm miss} > 0$ GeV and $|\vec{p}_{\rm miss}| > 0$ GeV/c, respectively, as they do not yield significant improvement on the resolution of n_X^2, and do not increase the ratio of signal to background events.

The final event sample contains about 22 % of background events. The background is composed of 12 % continuum and combinatorial background and 10 % decays of the signal B meson other than the semileptonic decay $\overline{B} \to X_c\ell^-\overline{\nu}$. Combinatorial and continuum background is subtracted using the sideband of the $m_{\rm ES}$ distribution, as described above. The residual background events, con-

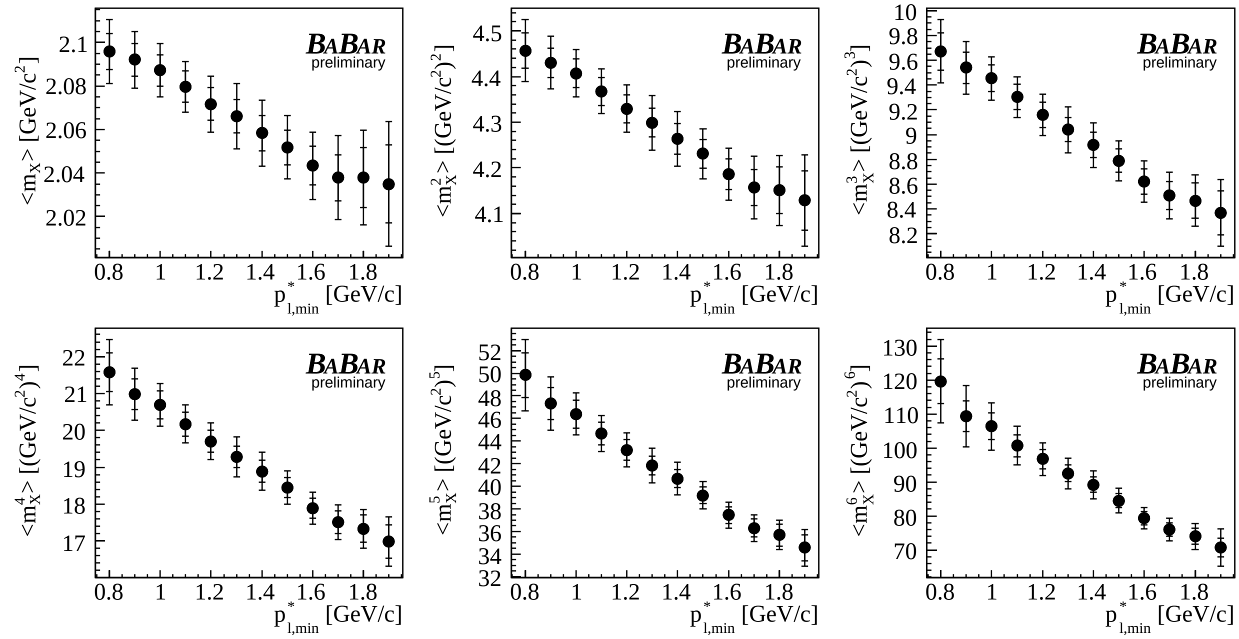

FIG. 5: Measured hadronic mass moments $\langle m_X^k \rangle$ with $k = 1 \ldots 6$ for different selection criteria on the minimal lepton momentum $p^*_{\ell,\mathrm{min}}$. The inner error bars correspond to the statistical uncertainties while the full error bars correspond to the total uncertainties. The moments are highly correlated.

taining a correctly reconstructed B_{reco} meson, are subtracted using MC simulations. The dominant sources are pions misidentified as muons, $\overline{B} \to X_u \ell^- \overline{\nu}$ decays, and secondary semileptonic decays of D and D_s mesons.

The measured n_X^2 spectra for cuts on the lepton momentum at $p^*_\ell \geq 0.8\,\mathrm{GeV}/c$ and $p^*_\ell \geq 1.9\,\mathrm{GeV}/c$ are shown together with the backgound distributions in Fig. 6. We measure 7827 ± 108 (1278 ± 42) signal events for $p^*_\ell \geq 0.8$ $(1.9)\,\mathrm{GeV}/c$, respectively.

A. Extraction of Moments

To extract unbiased moments $\langle n_X^k \rangle$, effects that distort the n_X^2 distribution need to be corrected. These are the limited detector acceptance, resulting in a loss of particles, the resolution of measured charged particle momenta and energy depositions in the EMC, as well as the radiation of final-state photons. These photons are included in the measured X_c system and thus lead to a modified energy and mass measurement of the inclusive system. In the case of radiation from the lepton, the lepton's measured momentum is also lowered w.r.t. its initial momentum. The measured moments are corrected for the impact of these photons.

As described before, we find linear relationships correcting the measured means $\langle n^k_{X\,\mathrm{reco}} \rangle$ to the true means $\langle n^k_{X\,\mathrm{true}} \rangle$ described by first order polynomials. These functions vary with the measured lepton momentum, the measured $E_{\mathrm{miss}} - c|\vec{p}_{\mathrm{miss}}|$, and the measured multiplicity of the inclusive X_c system. The curves are therefore derived in three bins of $E_{\mathrm{miss}} - c|\vec{p}_{\mathrm{miss}}|$ and three bins of the multiplicity for each of the 12 lepton momentum bins of 100 MeV/c. We also find differences for events containing an electron or a muon and therefore derive separate correction functions for these two classes of events. The measured n_X^k value is corrected on an event-by-event basis using the inverse of these functions:

$$n^k_{X,\mathrm{calib}} = \frac{n^k_{X,\mathrm{reco}} - A(E_{\mathrm{miss}} - c|\vec{p}_{\mathrm{miss}}|, N_{X_c}, k, p^*_\ell)}{B(E_{\mathrm{miss}} - c|\vec{p}_{\mathrm{miss}}|, N_{X_c}, k, p^*_\ell)}. \quad (5)$$

Here A and B are the offset and the slope of the calibration function and differ for each order $k = 2, 4, 6$ and for each of the abovementioned bins. Figure 7 shows calibration curves for the moments $\langle n_X^k \rangle$ $(k = 2, 4, 6)$, integrated over all multiplicity bins and bins in $E_{\mathrm{miss}} - c|\vec{p}_{\mathrm{miss}}|$, for three different bins of p^*_ℓ. These calibration curves are extracted separately for events containing an electron or muon. Differences are mainly visible in the low momentum bin.

To verify this calibration procedure, we extract the moments of n_X^k of individual exclusive $\overline{B} \to X_c \ell^- \overline{\nu}$ modes on a MC sample and compare the calibrated moments to the true moments. The result of this study for the moments $\langle n_X^2 \rangle$ is plotted in Fig. 8, confirming that the extraction method is able to reproduce the true moments. Small biases remaining after calibration are of the order of $1\,\%$ for $\langle n_X^2 \rangle$ and in the order of few percent for $\langle n_X^4 \rangle$ and $\langle n_X^6 \rangle$ and are corrected and treated in the systematic uncertainties.

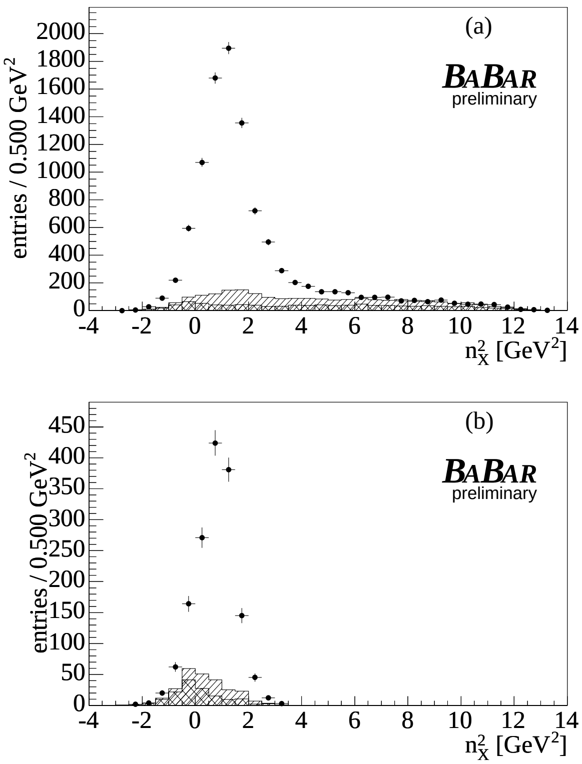

FIG. 6: Spectra of n_X^2 after the kinematic fit together with distributions of combinatorial background and background from non-$B\overline{B}$ decays (hatched area) as well as residual background (crossed area) for different minimal lepton momenta $p_\ell^* \geq 0.8\,\mathrm{GeV}/c$ (a) and $p_\ell^* \geq 1.9\,\mathrm{GeV}/c$ (b).

Background contributions are subtracted applying n_X^2 dependent weight factors $w_i(n_X^2)$ on an event-by-event basis, leading to the following expression for the moments:

$$\langle n_X^k \rangle = \frac{\sum_{i=1}^{N_{\mathrm{ev}}} w_i(n_X^2) \cdot n_{X\,\mathrm{calib},i}^k}{\sum_{i=1}^{N_{\mathrm{ev}}} w_i(n_X^2)} \times \mathcal{C}(p_\ell^*, k) \qquad (6)$$

The bias correction factor $\mathcal{C}(p_\ell^*, k)$ depends on the minimal lepton momentum and the order of the extracted moments. It is derived on MC simulations and corrects for the small bias remaining after the calibration.

B. Systematic Studies

The main sources of systematic uncertainties have been identified as the simulation of the detector efficiency to detect neutral clusters. The corresponding effect from charged tracks is smaller but still contributes to the uncertainty on the moments. Their impact has been evaluated by randomly excluding neutral or charged candidates from the X_c system with a probability of 1.8 % for the neutral candidates and 0.8% for the charged tracks, corresponding to the systematic uncertainties of the efficiency extraction methods. For the tracks we add in quadrature the statistical uncertainties from the control samples to the 0.8 % systematic uncertainty. The uncertainty arising from the differences between data and MC in the $E_{\mathrm{miss}} - c|\vec{p}_{\mathrm{miss}}|$ distributions is evaluated by changing the selected region of $E_{\mathrm{miss}} - c|\vec{p}_{\mathrm{miss}}|$ to [0.0,0.2] GeV and [0.0, 0.4] GeV. To evaluate the uncertainty due to the binning of the calibration curves in the multiplicity, we randomly increase the measured multiplicity used for the choice of the calibration curve by one with a probability of 5% corresponding to observed differences between data and MC.

Smaller uncertainties arise from the unknown branching fractions of the background decay modes. Their branching fractions are scaled to agree with recent measurements [26] and are varied within their uncertainties. The MC sample is corrected for differences in the identification efficiencies between data and MC for various particle types. The uncertainty on the background due to pions misidentified as muons is evaluated by changing the MC corrections within the statistical uncertainties of these data control samples. While the background shape does not vary, the amount decreases up to 8 %. For the estimate of the uncertainty due to particle identification, we propagate this variation into the extracted moments.

A similar variation procedure is applied for the branching fractions of the exclusive signal modes, varying them several times randomly within 10 % for the D^*, 15 % for the D, 50 % for the individual D^{**} modes and 75% for the non-resonant modes. The inclusive rate for the decays $\overline{B} \to X_c \ell^- \overline{\nu}$ is conserved by rescaling all other modes. In addition, all D^{**} (non-resonant) modes are scaled in common, again randomly within 50%, keeping the inclusive decay rate $\overline{B} \to X_c \ell^- \overline{\nu}$ constant by rescaling the non-resonant (D^{**}) modes only. Experimental uncertainties on the signal branching fractions are fully covered by these variations [26]. This dependence of the extraction method results in changes of the calibration curve and bias correction, however the impact on the moments measured on data is small. We conservatively add half of the bias correction remaining after calibration to the uncertainty related to the extraction method.

The stability of the results has been tested by splitting the data sample into several independent subsamples: $B^\pm$ and B^0, decays to electrons and muons, and different run periods of roughly equal data-sample sizes. No significant variations are observed.

C. Results

Figure 9 shows the results for the moments $\langle n_X^2 \rangle$, $\langle n_X^4 \rangle$, $\langle n_X^6 \rangle$, and the central moments $\langle (n_X^2 - \langle n_X^2 \rangle)^k \rangle$ and $\langle (n_X^2 - 1.35\ \mathrm{GeV}^2)^k \rangle$ for $k = 2$ and 3 as a function of the p_ℓ^* cut. The moments are highly correlated due to the overlapping data samples. The full numerical results

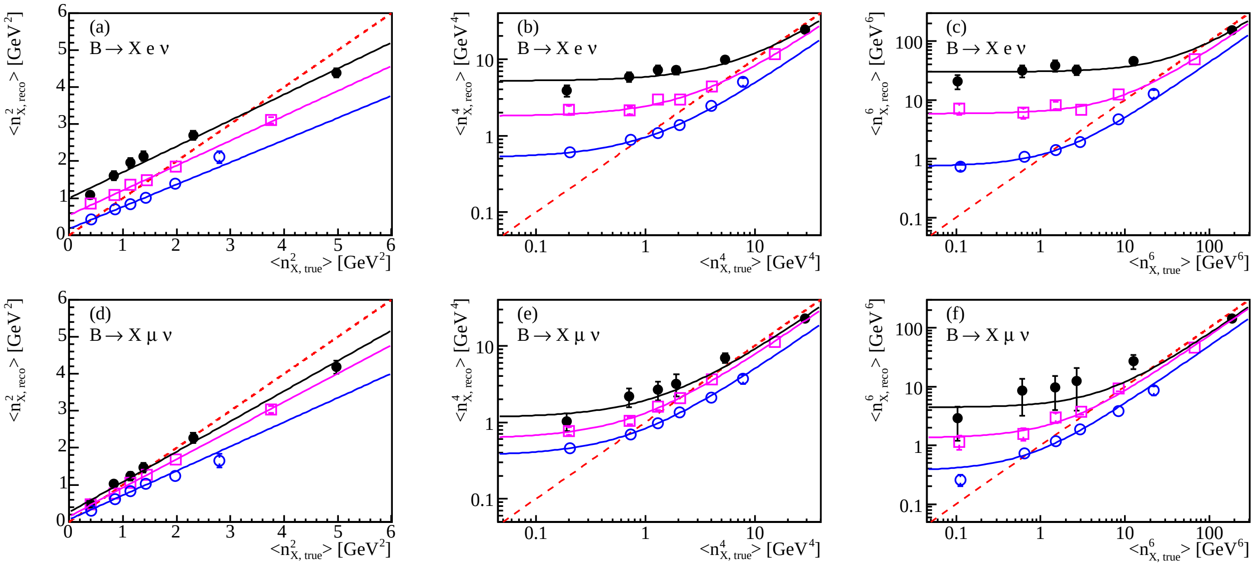

FIG. 7: Examples of calibration curves for $\langle n_X^k \rangle$ ($k = 2, 4, 6$) in bins of p_ℓ^*, extracted separately for events $\overline{B} \to X e \overline{\nu}$ (a)-(c) and $\overline{B} \to X \mu \overline{\nu}$ (d)-(f). Shown are the extracted $\langle n^k_{X,\mathrm{reco}} \rangle$ versus $\langle n^k_{X,\mathrm{true}} \rangle$ in bins of $n^2_{X\,\mathrm{true}}$ for $0.9 \leq p_\ell^* < 1.0\,\mathrm{GeV}/c$ (•), $1.4 \leq p_\ell^* < 1.5\,\mathrm{GeV}/c$ (□), and $p_\ell^* \geq 1.9\,\mathrm{GeV}/c$ (∘) integrated over multiplicity and $E_{\mathrm{miss}} - c|\vec{p}_{\mathrm{miss}}|$ bins. The results of fits of linear functions are overlaid as solid lines. Reference lines with $\langle n^k_{X,\mathrm{reco}} \rangle = \langle n^k_{X,\mathrm{true}} \rangle$ are superimposed (dashed lines). Please note the logarithmic scales in (b), (c), (e), and (f).

and the statistical and the estimated systematic uncertainties can be found in Tables A.III - A.VII. A clear dependence on the lepton momentum selection criteria is observed for all moments, due to the varying contributions from higher mass final states with decreasing lepton momentum. Statistical uncertainties on the moments $\langle n_X^k \rangle$ arise from the limited data sample, the width of the measured distribution $\langle n_X^{2k} \rangle - \langle n_X^k \rangle^2$, and limited statistics on the MC samples used for the extraction of background shapes, calibration curves, and bias correction. In most cases we obtain systematic uncertainties slightly exceeding the statistical uncertainty.

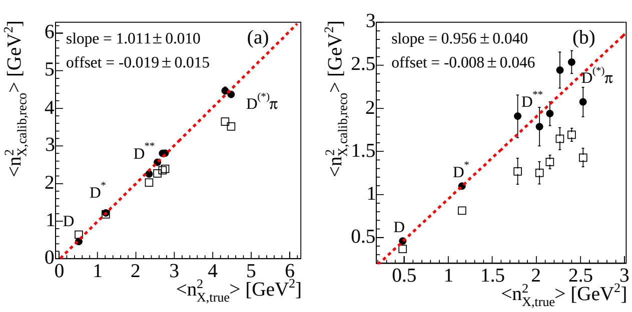

FIG. 8: Result of the calibration verification procedure for different minimal lepton momenta $p_\ell^* \geq 0.8\,\mathrm{GeV}/c$ (a) and $p_\ell^* \geq 1.9\,\mathrm{GeV}/c$ (b). Moments $\langle n_X^2 \rangle$ of exclusive modes on simulated events before calibration (□) and after calibration (•) plotted against the true moments for each mode. The dotted line shows the fit result to the calibrated moments, the resulting parameters are shown.

VI. DETERMINATION OF $|V_{cb}|$ AND THE QUARK MASSES m_b AND m_c

At the parton level, the weak decay rate for $b \to c\ell\nu$ can be calculated accurately; it is proportional to $|V_{cb}|^2$ and depends on the quark masses, m_b and m_c. To relate measurements of the semileptonic B-meson decay rate to $|V_{cb}|$, the parton-level calculations have to be corrected for effects of strong interactions. Heavy-Quark Expansions (HQEs) [27–29] have become a successful tool for calculating perturbative and non-perturbative QCD corrections [30–34] and for estimating their uncertainties.

In the kinetic-mass scheme [14, 35–39], these expansions in $1/m_b$ and $\alpha_s(m_b)$ (the strong coupling constant) to order $\mathcal{O}(1/m_b^3)$ contain six parameters: the running kinetic masses of the $b-$ and $c-$quarks, $m_b(\mu)$ and $m_c(\mu)$, and four non-perturbative parameters. The parameter μ denotes the Wilson normalization scale that separates effects from long- and short-distance dynamics. The calculations are performed for $\mu = 1\,\mathrm{GeV}$ [40]. We determine these six parameters from a fit to the moments of the hadronic-mass and electron-energy [6] distributions in semileptonic B decays $\overline{B} \to X_c \ell^- \overline{\nu}$ and moments of the photon-energy spectrum in decays $B \to X_s \gamma$ [10, 11].

In the kinetic-mass scheme the HQE to $\mathcal{O}(1/m_b^3)$ for the rate Γ_{SL} of semileptonic decays $\overline{B} \to X_c \ell^- \overline{\nu}$ can be expressed as [35]

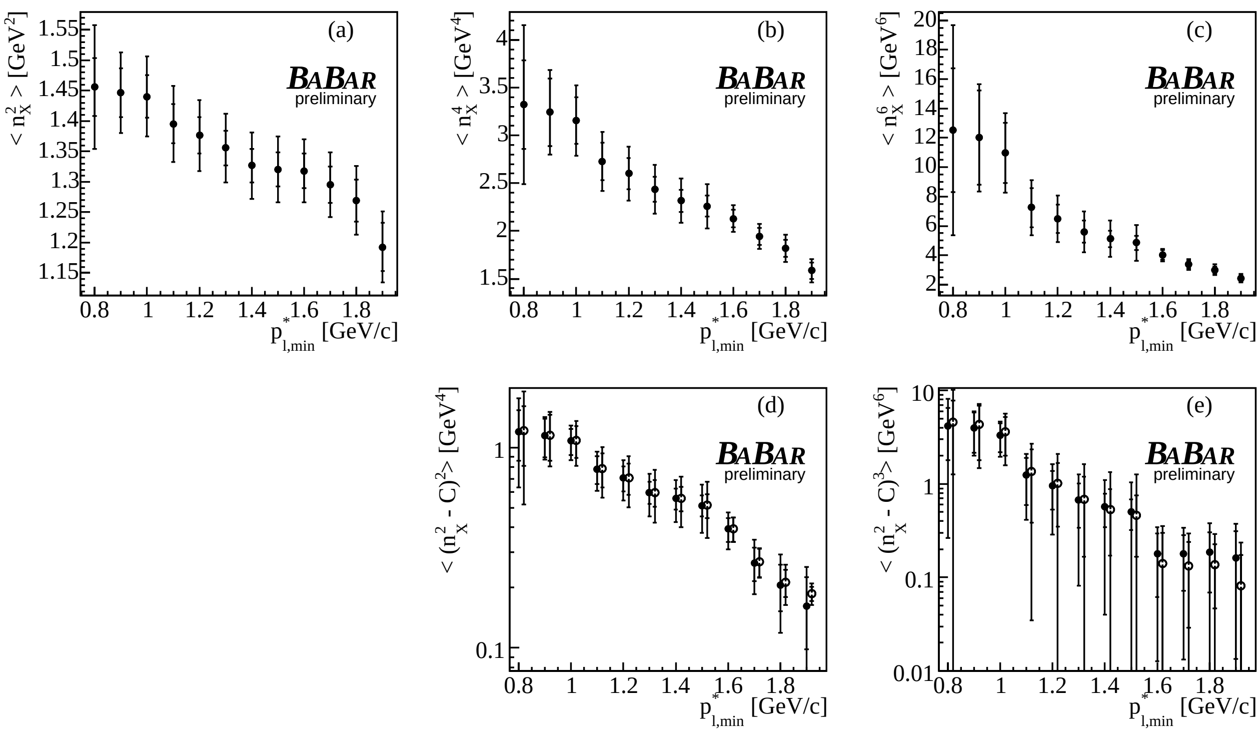

FIG. 9: Measured moments $\langle n_X^2\rangle$ (a), $\langle n_X^4\rangle$ (b), $\langle n_X^6\rangle$ (c), and the central moments $\langle (n_X^2 - C)^2\rangle$ with $C = \langle n_X^2\rangle$ (•) and $C = 1.35$ GeV^2 (○) (d), and $\langle (n_X^2 - C)^3\rangle$ with $C = \langle n_X^2\rangle$ (•) and $C = 1.35$ GeV^2 (○) (e) for different cuts on the lepton momentum p_ℓ^* . The error bars indicate the statistical and the total errors, respectively. Please note the logarithmic scale on the y-axis in plots (d) and (e). The moments are highly correlated.

$$
\begin{aligned}
\Gamma_{SL} &= \frac{G_F^2 m_b^5}{192\pi^3}|V_{cb}|^2(1+A_{ew})A_{pert}(r,\mu) \\
&\times \left[z_0(r)\left(1 - \frac{\mu_\pi^2 - \mu_G^2 + \frac{\rho_D^3+\rho_{LS}^3}{c^2 m_b}}{2c^4 m_b^2}\right) \right. \qquad (7) \\
&- \left. 2(1-r)^4 \frac{\mu_G^2 + \frac{\rho_D^3+\rho_{LS}^3}{c^2 m_b}}{c^4 m_b^2} + d(r)\frac{\rho_D^3}{c^6 m_b^3} + \mathcal{O}(1/m_b^4)\right].
\end{aligned}
$$

The leading non-perturbative effects arise at $\mathcal{O}(1/m_b^2)$ and are parameterized by $\mu_\pi^2(\mu)$ and $\mu_G^2(\mu)$, the expectation values of the kinetic and chromomagnetic dimension-five operators. At $\mathcal{O}(1/m_b^3)$, two additional parameters enter, $\rho_D^3(\mu)$ and $\rho_{LS}^3(\mu)$, the expectation values of the Darwin and spin-orbit dimension-six operators, respectively. The ratio $r = m_c^2/m_b^2$ enters in the tree level phase-space factor $z_0(r) = 1 - 8r + 8r^3 - r^4 - 12r^2 \ln r$ and in the function $d(r) = 8\ln r + 34/3 - 32r/3 - 8r^2 + 32r^3/3 - 10r^4/3$. The factor $1 + A_{ew}$ accounts for electroweak corrections. It is estimated to be $1 + A_{ew} \cong (1 + \alpha/\pi \ln M_Z/m_b)^2 = 1.014$. The quantity A_{pert} accounts for perturbative contributions and is estimated to be $A_{pert}(r,\mu) \approx 0.908$ [35].

The performed fit uses a linearized expression for the dependence of $|V_{cb}|$ on the values of heavy-quark parameters, expanded around *a priori* estimates of these parameters [35]:

$$
\begin{aligned}
\frac{|V_{cb}|}{0.0417} &= \sqrt{\frac{\mathcal{B}_{clv}}{0.1032}\frac{1.55}{\tau_B}} \\
&\times[1 + 0.30(\alpha_s(m_b) - 0.22)] \\
&\times[1 - 0.66(m_b - 4.60) + 0.39(m_c - 1.15) \\
&+0.013(\mu_\pi^2 - 0.40) + 0.09(\rho_D^3 - 0.20) \\
&+0.05(\mu_G^2 - 0.35) - 0.01(\rho_{LS}^3 + 0.15)]. \qquad (8)
\end{aligned}
$$

Here m_b and m_c are in GeV/c^2 and all other parameters of the expansion are in GeV^k; τ_B refers to the average lifetime of B mesons produced at the $\Upsilon(4S)$ and is given in ps. HQEs in terms of the same heavy-quark parameters are available for hadronic-mass, electron-energy, and photon-energy moments. Predictions for those moments are obtained from an analytical calculation. We use these calculations to determine $|V_{cb}|$, the total semileptonic branching fraction $\mathcal{B}$, the quark masses m_b and m_c, as well as the heavy-quark parameters μ_π^2, μ_G^2, ρ_D^3, and ρ_{LS}^3, from a simultaneous χ^2 fit to the measured moments and partial branching fractions, all as functions of the minimal lepton momentum $p_{\ell,\min}^*$ and minimal photon energies $E_{\gamma,\min}$.

A. Extraction Formalism

The fit method designed to extract the HQE parameters from the moments measurements has been reported previously [12, 41]. It is based on a χ^2 minimization,

$$\chi^2 = \left(\vec{M}_{\rm exp} - \vec{M}_{\rm HQE}\right)^T \mathcal{C}_{\rm tot}^{-1} \left(\vec{M}_{\rm exp} - \vec{M}_{\rm HQE}\right). \quad (9)$$

The vectors $\vec{M}_{\rm exp}$ and $\vec{M}_{\rm HQE}$ contain the measured moments included in the fit and the corresponding moments calculated by theory, respectively. Furthermore, the expression in Eq. 9 contains the total covariance matrix $\mathcal{C}_{\rm tot}$ defined as the sum of the experimental, $\mathcal{C}_{\rm exp}$, and theoretical, $\mathcal{C}_{\rm HQE}$, covariance matrices (see Section VI C).

The total semileptonic branching fraction, $\mathcal{B}(\overline{B} \to X_c\ell^-\overline{\nu})$, is extracted in the fit by extrapolating measured partial branching-fractions, $\mathcal{B}_{p^*_{\ell,\rm min}}(\overline{B} \to X_c\ell^-\overline{\nu})$, with $p^*_\ell \geq p^*_{\ell,\rm min}$ to the full lepton energy spectrum. Using HQE predictions of the relative decay fraction

$$R_{p^*_{\ell,\rm min}} = \frac{\int_{p^*_{\ell,\rm min}} \frac{{\rm d}\Gamma_{SL}}{{\rm d}E^*_\ell}{\rm d}E^*_\ell}{\int_0 \frac{{\rm d}\Gamma_{SL}}{{\rm d}E^*_\ell}{\rm d}E^*_\ell}, \quad (10)$$

the total branching fraction can be introduced as a free parameter in the fit. It is given by

$$\mathcal{B}(\overline{B} \to X_c\ell^-\overline{\nu}) = \frac{\mathcal{B}_{p^*_{\ell,\rm min}}(\overline{B} \to X_c\ell^-\overline{\nu})}{R_{p^*_{\ell,\rm min}}}. \quad (11)$$

The total branching fraction can be used together with the average B-meson lifetime τ_B to calculate the total semileptonic rate proportional to $|V_{cb}|^2$,

$$\Gamma_{SL} = \frac{\mathcal{B}(\overline{B} \to X_c\ell^-\overline{\nu})}{\tau_B} \propto |V_{cb}|^2. \quad (12)$$

By adding τ_B to the vectors of measured and predicted quantities, $\vec{M}_{\rm exp}$ and $\vec{M}_{\rm HQE}$, $|V_{cb}|$ can be extracted from the fit as an additional free parameter using Eq. 8.

The non-perturbative parameters μ^2_G and ρ^3_{LS} have been estimated from B-B^* mass splitting and heavy-quark sum rules to be $\mu^2_G = (0.35 \pm 0.07)\,{\rm GeV}^2$ and $\rho^3_{LS} = (-0.15 \pm 0.10)\,{\rm GeV}^3$ [12], respectively. Both parameters are restricted in the fit by imposing Gaussian error constraints.

B. Experimental Input

The combined fit is performed on a subset of available moment measurements with correlations below 95% to ensure the invertibility of the covariance matrix. Since the omitted measurements are characterized by high correlations to other measurements considered in the fit they do not contribute significant additional information and the overall sensitivity of the results is not affected. All results are based on the following set of moment measurements, 27 in total:

- Lepton energy moments measured by *BABAR* [6]. We use the partial branching fraction $\mathcal{B}_{p^*_{\ell,\rm min}}$ measured for $p^*_\ell \geq 0.6, 1.0, 1.5\,{\rm GeV}/c$ and the moments $\langle E_\ell\rangle$ for $p^*_\ell \geq 0.6, 0.8, 1.0, 1.2, 1.5\,{\rm GeV}/c$. The lepton energy moments $\langle E^2_\ell\rangle$ are used at the minimal lepton momentum $p^*_\ell \geq 0.6, 1.0, 1.5\,{\rm GeV}/c$ and $\langle E^3_\ell\rangle$ at $p^*_\ell \geq 0.8, 1.2\,{\rm GeV}/c$.

- Hadronic mass moments are used as presented in this paper. We select the following subset for the fit: $\langle m^2_X\rangle$ for $p^*_\ell \geq 0.9, 1.1, 1.3, 1.5\,{\rm GeV}/c$ and $\langle m^4_X\rangle$ for $p^*_\ell \geq 0.8, 1.0, 1.2, 1.4\,{\rm GeV}/c$.

- Photon energy moments measured in $B \to X_s\gamma$ decays are taken from [10] and [11]: $\langle E_\gamma\rangle$ for the minimal photon energy $E_\gamma \geq 1.9, 2.0\,{\rm GeV}$ and $\langle E^2_\gamma\rangle$ for $E_\gamma \geq 1.9\,{\rm GeV}$.

In addition we use $\tau_B = f_0\tau_0 + (1 - f_0)\tau_\pm = (1.585 \pm 0.007)\,{\rm ps}$, taking into account the lifetimes [26] of neutral and charged B mesons, τ_0 and $\tau_\pm$, and their relative production rates, $f_0 = 0.491 \pm 0.007$ [26], the fraction of $B^0\overline{B}^0$ pairs.

C. Theoretical Uncertainties

As discussed in [12] and specified in [14] the following theoretical uncertainties are taken into account:

The uncertainty related to the uncalculated perturbative corrections to the Wilson coefficients of non-perturbative operators are estimated by varying the corresponding parameters μ^2_π and μ^2_G by 20% and ρ^3_D and ρ^3_{LS} by 30% around their expected values.

Uncertainties for the perturbative corrections are estimated by varying $\alpha_s = 0.22$ up and down by 0.1 for the hadronic mass moments and by 0.04 for the lepton energy moments around its nominal value.

Uncertainties in the perturbative corrections of the quark masses m_b and m_c are addressed by varying both by $20\,{\rm MeV}/c^2$ up and down around their expected values.

For the extracted value of $|V_{cb}|$ an additional error of 1.4% is added for the uncertainty in the expansion of the semileptonic rate Γ_{SL} [35, 39]. It accounts for remaining uncertainties in the perturbative corrections to the leading operator, uncalculated perturbative corrections to the chromomagnetic and Darwin operator, higher order power corrections, and possible non-perturbative effects in the operators with charm fields. This uncertainty is not included in the theoretical covariance matrix $\mathcal{C}_{\rm HQE}$ but is listed separately as a theoretical uncertainty on $|V_{cb}|$.

For the predicted photon energy moments $\langle E^n_\gamma\rangle$, additional uncertainties are taken into account. As outlined in [36], additional uncertainties of 30% of the applied bias correction to the photon-energy moments and half the difference in the moments derived from two different distribution-function ansätze have to be considered. Both contributions are added linearly.

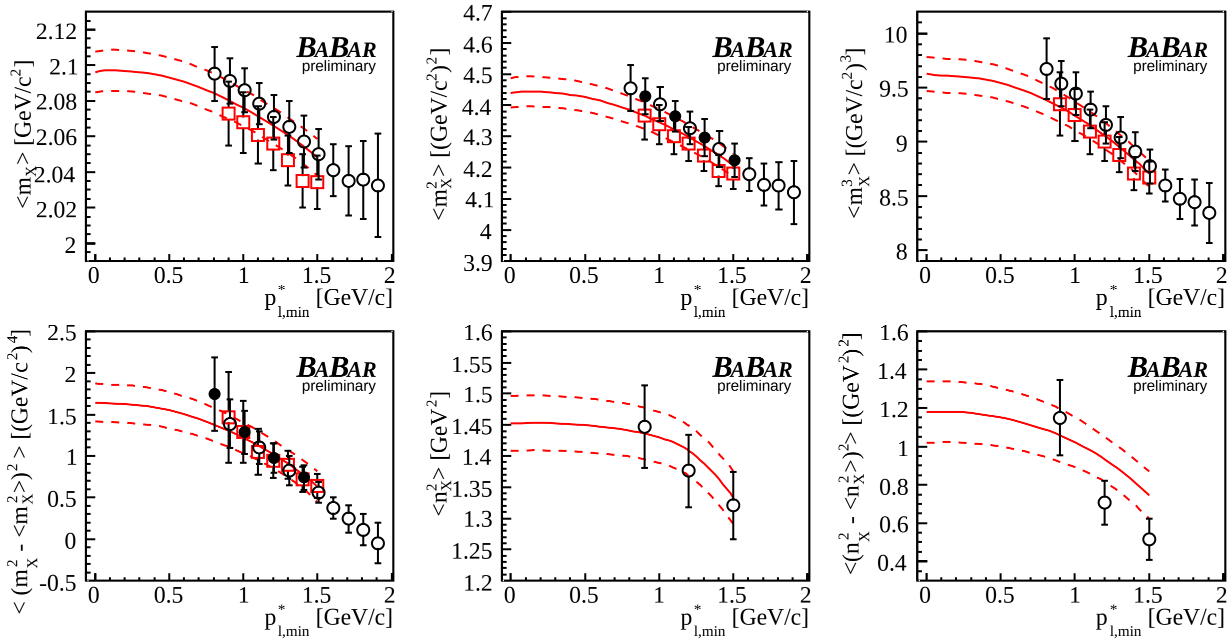

FIG. 10: The measured hadronic-mass and mixed moments (●/○), as a function of the minimal lepton momentum $p^*_{\ell,\min}$ compared with the result of the simultaneous fit (solid line) and a previous measurement by the *BABAR* Collaboration (□) [2]. The solid data points mark the measurements included in the fit. The vertical bars indicate the experimental errors. The dashed lines correspond to the total fit uncertainty as obtained by converting the fit errors of each individual HQE parameter into an error for the individual moment.

The theoretical covariance matrix $\mathcal{C}_{\rm HQE}$ is constructed by assuming fully correlated theoretical uncertainties for a given moment with different lepton momentum or photon energy cutoff and assuming uncorrelated theoretical uncertainties for moments of different orders and types. The additonal uncertainties considered for the photon energy moments are assumed to be uncorrelated for different moments and photon energy cutoffs.

D. Results

A comparison of the fit results for the hadronic-mass and mixed moments with the measured moments is shown in Fig. 10. The moments $\langle m_X \rangle$ and $\langle m_X^3 \rangle$ are not included in the fit and thus provide an unbiased comparison with the fitted HQE prediction. We find an overall good agreement, also indicated by $\chi^2 = 8$ for 20 degrees of freedom. The measured moments continue to decrease with increasing $p^*_{\ell,\min}$ and extend beyond theoretical predictions available for $p^*_{\ell,\min} \leq 1.5\,\mathrm{GeV}/c$.

Comparing the measured moments $\langle n_X^2 \rangle$ and $\langle (n_X^2 - \langle n_X^2 \rangle)^2 \rangle$ with predictions resulting from the presented fit, a good agreement is found. The calculations used for the predictions of the mixed moments are currently missing $p^*_{\ell,\min}$-dependent perturbative corrections. The $p^*_{\ell,\min}$ dependence of the perturbative corrections for those moments is however expected to be small [38].

The fit results for the standard model and HQE parameters are summarized in Table I. We find as preliminary results $|V_{cb}| = (41.88 \pm 0.81) \cdot 10^{-3}$ and $m_b = (4.552 \pm 0.055)\,\mathrm{GeV}/c^2$. The results are in good agreement with earlier determinations [12, 13], showing slightly increased uncertainties due to the limited experimental input used in this fit.

Figure 11 shows the $\Delta\chi^2 = 1$ contours in the $(m_b, |V_{cb}|)$ and (m_b, μ_π^2) planes. It compares the standard fit including photon energy moments, and a fit based on moments from semileptonic $\overline{B} \to X_c \ell^- \overline{\nu}$ decays only, clearly indicating the significance of the constraints from the $B \to X_s \gamma$ decays for both $|V_{cb}|$ and m_b.

VII. SUMMARY

We have reported preliminary results for the moments $\langle m_X^k \rangle$ with $k = 1, \ldots, 6$ of the hadronic mass distribution in semileptonic B-meson decays to final states containing a charm quark. In addition we have presented preliminary results for a first measurement of the moments $\langle n_X^k \rangle$ for $k = 2, 4, 6$ with n_X^2 a combination of mass and energy of the hadronic system X_c. The results for the mass moments agree with the previous measurements [1–5] but tend in general to higher values, between 1% and 2% for $\langle m_X \rangle$ and $\langle m_X^4 \rangle$, respectively, relative to the previous *BABAR* measurement [2]. The increased data sample compared to the previous *BABAR* measurement led

TABLE I: Fit results with experimental and theoretical uncertainties. For $|V_{cb}|$ we take an additional theoretical uncertainty of 1.4% from the uncertainty in the expansion of Γ_{SL} into account. Correlations coefficients for all parameters are summarized below the results.

	$\lvert V_{cb}\rvert \times 10^3$	m_b [GeV/c^2]	m_c [GeV/c^2]	$\mathcal{B}$ [%]	μ_π^2 [GeV^2]	μ_G^2 [GeV^2]	ρ_D^3 [GeV^3]	ρ_{LS}^3 [GeV^3]
Results	41.88	4.552	1.070	10.597	0.471	0.330	0.220	-0.159
Δ_{exp}	0.44	0.038	0.055	0.171	0.034	0.042	0.021	0.081
Δ_{theo}	0.35	0.040	0.065	0.053	0.062	0.043	0.042	0.050
$\Delta\Gamma_{SL}$	0.59							
Δ_{tot}	0.81	0.055	0.085	0.179	0.070	0.060	0.047	0.095
$\lvert V_{cb}\rvert$	1.00	-0.42	-0.27	0.75	0.42	-0.28	0.25	0.10
m_b		1.00	0.96	0.09	-0.56	-0.07	-0.38	-0.24
m_c			1.00	0.15	-0.63	-0.32	-0.51	-0.15
$\mathcal{B}$				1.00	0.09	-0.10	0.02	-0.04
μ_π^2					1.00	0.40	0.87	0.10
μ_G^2						1.00	0.41	-0.05
ρ_D^3							1.00	-0.21
ρ_{LS}^3								1.00

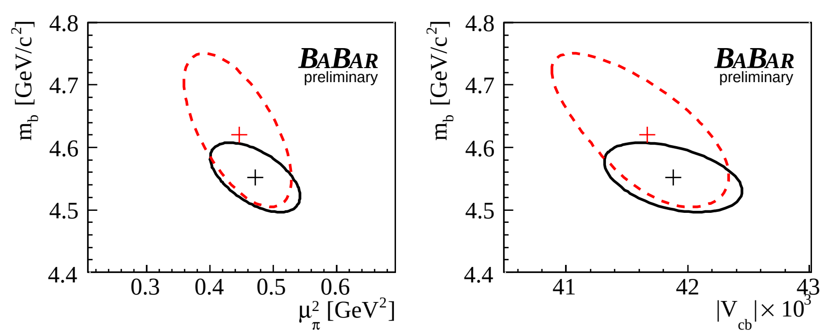

FIG. 11: $\Delta\chi^2 = 1$ contours for the fit results in the $(m_b, |V_{cb}|)$ and (m_b, μ_π^2) planes comparing the results of the presented fit (black line) with those of a fit omitting the photon-energy moments (red dashed line).

to significantly smaller statistical uncertainties which are smaller than the systematic uncertainties.

We have made a combined fit in the kinetic scheme to the hadronic mass moments, measured moments of the lepton-energy spectrum [6], and moments of the photon energy spectrum in decays $B \to X_s\gamma$ [10, 11]. The combined fit yields preliminary results for $|V_{cb}|$, the quark masses m_b and m_c, the total semileptonic branching fraction $\mathcal{B}(\overline{B} \to X_c\ell^-\overline{\nu})$, and the dominant non-perturbative HQE parameters in agreement with previous determinations. We obtain $|V_{cb}| = (41.88 \pm 0.81) \cdot 10^{-3}$ and $m_b = (4.552 \pm 0.055)\,\mathrm{GeV}/c^2$.

We are grateful for the extraordinary contributions of our PEP-II colleagues in achieving the excellent luminosity and machine conditions that have made this work possible. The success of this project also relies critically on the expertise and dedication of the computing organizations that support *BABAR*. The collaborating institutions wish to thank SLAC for its support and the kind hospitality extended to them. This work is supported by the US Department of Energy and National Science Foundation, the Natural Sciences and Engineering Research Council (Canada), the Commissariat à l'Energie Atomique and Institut National de Physique Nucléaire et de Physique des Particules (France), the Bundesministerium für Bildung und Forschung and Deutsche Forschungsgemeinschaft (Germany), the Istituto Nazionale di Fisica Nucleare (Italy), the Foundation for Fundamental Research on Matter (The Netherlands), the Research Council of Norway, the Ministry of Science and Technology of the Russian Federation, Ministerio de Educación y Ciencia (Spain), and the Science and Technology Facilities Council (United Kingdom). Individuals have received support from the Marie-Curie IEF program (European Union) and the A. P. Sloan Foundation.

[1] S. E. Csorna *et al.* (CLEO Collaboration), Phys. Rev. D **70**, 032002 (2004).
[2] B. Aubert *et al.* (*BABAR* Collaboration), Phys. Rev. D **69**, 111103 (2004).
[3] D. Acosta *et al.* (CDF Collaboration), Phys. Rev. D **71**, 051103 (2005).
[4] J. Abdallah *et al.* (DELPHI Collaboration), Eur. Phys. J. C **45**, 35 (2006).
[5] C. Schwanda *et al.* (Belle Collaboration), Phys. Rev. D **75**, 032005 (2007).
[6] B. Aubert *et al.* (*BABAR* Collaboration), Phys. Rev. D **69**, 111104 (2004).
[7] K. Abe *et al.* (Belle Collaboration), hep-ex/0508056 (2005).
[8] S. Chen *et al.* (CLEO Collaboration), Phys. Rev. Lett. **87**, 251807 (2001).
[9] P. Koppenburg *et al.* (Belle Collaboration), Phys. Rev. Lett. **93**, 061803 (2004).
[10] B. Aubert *et al.* (*BABAR* Collaboration), Phys. Rev. D **72**, 052004 (2005).
[11] B. Aubert *et al.* (*BABAR* Collaboration), Phys. Rev. Lett. **97**, 171803 (2006).
[12] O. Buchmüller and H. Flächer, Phys. Rev. D **73**, 073008 (2006).
[13] C. W. Bauer *et al.*, Phys. Rev. D **70**, 094017 (2004).
[14] P. Gambino and N. Uraltsev, Eur. Phys. J. C **34**, 181 (2004).
[15] B. Aubert *et al.* (*BABAR* Collaboration), Nucl. Instrum. Meth. A **479**, 1 (2002).
[16] PEP-II: An Asymmetric B Factory. Conceptual Design Report, SLAC-R-418 (1993).
[17] S. Agostinelli *et al.* (GEANT4 Collaboration), Nucl. Instrum. Meth. A **506**, 250 (2003).
[18] D. J. Lange, Nucl. Instrum. Meth. A **462**, 152 (2001).
[19] E. Richter-Was, Phys. Lett. B **303**, 163 (1993).
[20] J. E. Duboscq *et al.* (CLEO Collaboration), Phys. Rev. Lett. **76**, 3898 (1996).
[21] D. Scora and N. Isgur, Phys. Rev. D **52**, 2783 (1995).
[22] J. L. Goity and W. Roberts, Phys. Rev. D **51**, 3459 (1995).
[23] B. Aubert *et al.* (*BABAR* Collaboration), Phys. Rev. Lett. **92**, 071802 (2004).
[24] H. Albrecht *et al.* (ARGUS Collaboration), Phys. Lett. B **185**, 218 (1987).
[25] T. Skwarnicki (Crystal Ball Collaboration), DESY F31-86-02 (1986).
[26] W.-M. Yao *et al.* (Particle Data Group (PDG)), Journal of Physics G **33**, 1 (2006), URL http://pdg.lbl.gov.
[27] M. Voloshin and M. Shifman, Sov. J. Nucl. Phys. **41**, 120 (1985).
[28] J. Chay, H. Georgi, and B. Grinstein, Phys. Lett. B **247**, 399 (1990).
[29] I. I. Y. Bigi and N. G. Uraltsev, Phys. Lett. B **280**, 271 (1992).
[30] I. I. Bigi, N. Uraltsev, and A. I. Vainshtein, Phys. Lett. B **293** (1992).
[31] I. I. Bigi, M. Shifman, N. G. Uraltsev, and A. Vainshtein, Phys. Rev. Lett. **71**, 496 (1993).
[32] B. Blok, L. Koyrakh, M. Shifman, and A. I. Vainshtein, Phys. Rev. D **49**, 3356 (1994).
[33] A. V. Manohar and M. B. Wise, Phys. Rev. D **49**, 1310 (1994).
[34] M. Gremm and A. Kapustin, Phys. Rev. D **55**, 6924 (1997).
[35] D. Benson, I. I. Bigi, T. Mannel, and N. Uraltsev, Nucl. Phys. **B665**, 367 (2003).
[36] D. Benson, I. I. Bigi, and N. Uraltsev, Nucl. Phys. **B710**, 371 (2005).
[37] V. Aquila, P. Gambino, G. Ridolfi, and N. Uraltsev, Nucl. Phys. **B719**, 77 (2005).
[38] N. Uraltsev, Int. J. Mod. Phys. A **20**, 2099 (2005).
[39] I. I. Bigi, N. Uraltsev, and R. Zwicky, Eur. Phys. J. C **50**, 539 (2007).
[40] I. Bigi, M. Shifman, N. Uraltsev, and A. Vainshtein, Phys. Rev. D **56**, 4017 (1997).
[41] B. Aubert *et al.* (*BABAR* Collaboration), Phys. Rev. Lett. **93**, 011803 (2004).

TABLE A.I: Results for the moments $\langle m_X^k \rangle$ with $k = 1 \ldots 3$ for different cuts on the minimal lepton momentum p_ℓ^* with absolute statistical and systematic uncertainties. Individual errors sources are specified due to modeling of the signal events, the calibration procedure, the background subtraction, detector efficiencies and resolution, and stability of moment measurements. Minimum lepton momenta cuts are given in GeV/c. Moments and uncertainties are given in $(\text{GeV}/c^2)^k$.

k	$p_{l,min}$	$\langle m_X^k \rangle$	σ_{stat}	σ_{sys}	Signal Model	$\mathcal{C}_{\text{calib}}$	BG subtr.	Detector	Stability
1	0.8	2.0958	±0.0083	±0.0121	0.0045	0.0042	0.0044	0.0095	0.0000
	0.9	2.0920	±0.0075	±0.0107	0.0039	0.0040	0.0042	0.0082	0.0000
	1.0	2.0872	±0.0072	±0.0099	0.0038	0.0041	0.0041	0.0070	0.0009
	1.1	2.0796	±0.0072	±0.0093	0.0036	0.0035	0.0041	0.0066	0.0000
	1.2	2.0717	±0.0075	±0.0104	0.0035	0.0047	0.0043	0.0067	0.0032
	1.3	2.0661	±0.0078	±0.0128	0.0032	0.0054	0.0045	0.0067	0.0077
	1.4	2.0583	±0.0081	±0.0128	0.0028	0.0059	0.0048	0.0065	0.0075
	1.5	2.0518	±0.0080	±0.0121	0.0025	0.0063	0.0053	0.0071	0.0045
	1.6	2.0433	±0.0089	±0.0128	0.0025	0.0077	0.0060	0.0079	0.0000
	1.7	2.0378	±0.0105	±0.0162	0.0024	0.0075	0.0073	0.0080	0.0091
	1.8	2.0379	±0.0139	±0.0168	0.0025	0.0070	0.0089	0.0096	0.0075
	1.9	2.0350	±0.0179	±0.0225	0.0020	0.0098	0.0121	0.0121	0.0107
2	0.8	4.457	±0.038	±0.056	0.022	0.016	0.018	0.046	0.000
	0.9	4.430	±0.032	±0.048	0.020	0.014	0.016	0.038	0.000
	1.0	4.407	±0.032	±0.041	0.019	0.014	0.015	0.030	0.000
	1.1	4.368	±0.031	±0.039	0.018	0.011	0.014	0.029	0.000
	1.2	4.330	±0.031	±0.041	0.017	0.016	0.014	0.027	0.015
	1.3	4.299	±0.032	±0.051	0.015	0.018	0.015	0.027	0.033
	1.4	4.263	±0.033	±0.049	0.014	0.020	0.016	0.026	0.031
	1.5	4.231	±0.031	±0.045	0.012	0.021	0.018	0.027	0.019
	1.6	4.186	±0.034	±0.046	0.012	0.026	0.020	0.031	0.000
	1.7	4.157	±0.040	±0.056	0.011	0.024	0.024	0.031	0.030
	1.8	4.151	±0.051	±0.058	0.011	0.022	0.029	0.036	0.025
	1.9	4.128	±0.065	±0.077	0.008	0.035	0.040	0.045	0.031
3	0.8	9.67	±0.15	±0.21	0.09	0.05	0.06	0.17	0.00
	0.9	9.54	±0.13	±0.17	0.08	0.04	0.05	0.14	0.00
	1.0	9.45	±0.11	±0.14	0.07	0.04	0.04	0.10	0.00
	1.1	9.30	±0.10	±0.13	0.07	0.03	0.04	0.10	0.00
	1.2	9.16	±0.10	±0.13	0.07	0.04	0.04	0.09	0.04
	1.3	9.04	±0.10	±0.16	0.06	0.05	0.04	0.08	0.11
	1.4	8.92	±0.10	±0.15	0.05	0.05	0.04	0.08	0.10
	1.5	8.79	±0.09	±0.13	0.05	0.05	0.05	0.08	0.06
	1.6	8.62	±0.10	±0.13	0.04	0.06	0.05	0.09	0.00
	1.7	8.51	±0.11	±0.15	0.04	0.06	0.06	0.09	0.07
	1.8	8.47	±0.14	±0.15	0.04	0.05	0.07	0.10	0.05
	1.9	8.37	±0.18	±0.20	0.03	0.10	0.10	0.13	0.06

TABLE A.II: Results for the moments $\langle m_X^k \rangle$ with $k = 4 \ldots 6$ for different cuts on the minimal lepton momentum p_ℓ^* with absolute statistical and systematic uncertainties. Individual errors sources are specified due to modeling of the signal events, the calibration procedure, the background subtraction, detector efficiencies and resolution, and stability of moment measurements. Minimum lepton momenta cuts are given in GeV/c. Moments and uncertainties are given in $(\text{GeV}/c^2)^k$.

k	$p_{l,min}$	$\langle m_X^k \rangle$	σ_{stat}	σ_{sys}	Signal Model	$\mathcal{C}_{\text{calib}}$	BG subtr.	Detector	Stability
4	0.8	21.58	±0.52	±0.72	0.30	0.12	0.21	0.61	0.00
	0.9	20.98	±0.41	±0.58	0.26	0.09	0.15	0.48	0.00
	1.0	20.69	±0.37	±0.44	0.26	0.09	0.12	0.32	0.00
	1.1	20.17	±0.33	±0.40	0.24	0.06	0.11	0.29	0.00
	1.2	19.70	±0.30	±0.39	0.23	0.09	0.10	0.26	0.13
	1.3	19.28	±0.29	±0.46	0.19	0.10	0.10	0.23	0.32
	1.4	18.89	±0.29	±0.43	0.17	0.11	0.10	0.22	0.29
	1.5	18.45	±0.27	±0.36	0.15	0.12	0.11	0.23	0.18
	1.6	17.89	±0.27	±0.34	0.13	0.14	0.12	0.25	0.00
	1.7	17.51	±0.31	±0.37	0.12	0.13	0.14	0.25	0.14
	1.8	17.33	±0.38	±0.37	0.11	0.11	0.17	0.27	0.09
	1.9	16.98	±0.46	±0.49	0.08	0.24	0.24	0.34	0.04
5	0.8	49.83	±1.97	±2.47	1.02	0.40	0.70	2.10	0.00
	0.9	47.33	±1.40	±1.91	0.90	0.22	0.47	1.60	0.00
	1.0	46.40	±1.23	±1.39	0.87	0.21	0.36	1.00	0.00
	1.1	44.67	±1.01	±1.23	0.80	0.10	0.29	0.87	0.00
	1.2	43.22	±0.93	±1.15	0.74	0.19	0.25	0.75	0.35
	1.3	41.84	±0.82	±1.32	0.62	0.21	0.24	0.64	0.92
	1.4	40.69	±0.82	±1.21	0.54	0.23	0.23	0.59	0.84
	1.5	39.21	±0.73	±0.99	0.45	0.25	0.25	0.60	0.53
	1.6	37.46	±0.73	±0.88	0.39	0.30	0.27	0.68	0.00
	1.7	36.31	±0.78	±0.89	0.35	0.25	0.32	0.66	0.26
	1.8	35.68	±0.96	±0.87	0.31	0.20	0.39	0.68	0.00
	1.9	34.57	±1.14	±1.17	0.23	0.58	0.53	0.84	0.00
6	0.8	119.64	±6.56	±10.42	4.19	6.19	2.28	6.89	0.00
	0.9	109.40	±4.49	±7.80	3.85	4.13	1.43	5.19	0.00
	1.0	106.41	±3.85	±5.80	3.83	2.86	1.03	3.11	0.00
	1.1	100.70	±3.22	±4.73	3.34	1.87	0.80	2.66	0.00
	1.2	96.71	±2.75	±3.99	2.95	1.47	0.60	2.17	0.00
	1.3	92.56	±2.45	±3.77	2.43	1.07	0.55	1.67	2.01
	1.4	89.20	±2.28	±3.42	2.10	0.65	0.54	1.67	1.94
	1.5	84.54	±1.99	±3.03	1.84	0.58	0.56	1.63	1.58
	1.6	79.35	±1.90	±2.53	1.62	0.60	0.61	1.75	0.00
	1.7	76.01	±2.01	±2.58	1.73	0.46	0.71	1.68	0.37
	1.8	73.97	±2.34	±3.07	2.41	0.35	0.87	1.66	0.00
	1.9	70.67	±2.71	±4.76	3.91	1.34	1.17	2.04	0.00

TABLE A.III: Results for $\langle n_X^k \rangle$ for $k = 2, 4, 6$ for all cuts p_ℓ^*. The systematic uncertainties are grouped in four categories having related sources: *rec. efficiency* is the sum of neutral and charged reconstruction efficiency differences data/MC, *data/MC mismod.* contains the errors from $E_{\rm miss} - c|\vec{p}_{\rm miss}|$ differences and multiplicity differences, *$\mathcal{B}$ bg. decays* sums all contributions from the variation of the residual background component (including the fake lepton background), and *signal model* sums the impact of the variation of the signal decay branching fractions and the error related to the bias correction.

k	p_ℓ^* [GeV/c]	$\langle n_X^k \rangle$	$\sigma_{\rm stat.}$	$\sigma_{\rm sys.}$	rec. efficiency	data/MC mismod.	$\mathcal{B}$ bg. decays	signal model
2	0.8	1.456	± 0.048	± 0.090	0.054	0.071	0.010	0.009
	0.9	1.447	± 0.040	± 0.053	0.038	0.035	0.010	0.006
	1.0	1.440	± 0.035	± 0.056	0.042	0.035	0.008	0.008
	1.1	1.395	± 0.032	± 0.054	0.038	0.035	0.006	0.014
	1.2	1.376	± 0.030	± 0.051	0.035	0.034	0.004	0.012
	1.3	1.356	± 0.029	± 0.049	0.032	0.034	0.004	0.011
	1.4	1.327	± 0.027	± 0.047	0.032	0.034	0.004	0.009
	1.5	1.321	± 0.028	± 0.046	0.030	0.033	0.004	0.008
	1.6	1.318	± 0.028	± 0.044	0.027	0.034	0.004	0.007
	1.7	1.295	± 0.030	± 0.044	0.027	0.034	0.005	0.006
	1.8	1.270	± 0.035	± 0.045	0.028	0.034	0.006	0.006
	1.9	1.193	± 0.040	± 0.043	0.021	0.033	0.007	0.015
4	0.8	3.32	± 0.46	± 0.69	0.34	0.59	0.08	0.12
	0.9	3.24	± 0.35	± 0.26	0.17	0.16	0.07	0.10
	1.0	3.15	± 0.25	± 0.27	0.19	0.16	0.05	0.11
	1.1	2.73	± 0.20	± 0.24	0.13	0.16	0.04	0.12
	1.2	2.60	± 0.16	± 0.23	0.11	0.16	0.01	0.12
	1.3	2.44	± 0.13	± 0.22	0.09	0.16	0.02	0.11
	1.4	2.32	± 0.12	± 0.20	0.07	0.16	0.01	0.10
	1.5	2.26	± 0.11	± 0.21	0.08	0.16	0.01	0.11
	1.6	2.13	± 0.09	± 0.10	0.06	0.07	0.00	0.05
	1.7	1.94	± 0.09	± 0.10	0.05	0.07	0.00	0.05
	1.8	1.82	± 0.09	± 0.11	0.06	0.06	0.00	0.06
	1.9	1.58	± 0.09	± 0.08	0.05	0.06	0.00	0.03
6	0.8	12.52	± 4.21	± 5.80	2.83	4.95	0.63	0.82
	0.9	12.00	± 3.21	± 1.74	1.13	1.05	0.55	0.59
	1.0	10.98	± 2.05	± 1.75	1.22	1.04	0.35	0.61
	1.1	7.25	± 1.34	± 1.32	0.63	1.04	0.22	0.47
	1.2	6.48	± 0.97	± 1.25	0.54	1.03	0.09	0.46
	1.3	5.60	± 0.75	± 1.17	0.35	1.03	0.08	0.41
	1.4	5.12	± 0.56	± 1.09	0.17	1.03	0.03	0.33
	1.5	4.85	± 0.49	± 1.11	0.19	1.02	0.02	0.39
	1.6	4.02	± 0.32	± 0.28	0.16	0.18	0.02	0.15
	1.7	3.38	± 0.26	± 0.25	0.12	0.18	0.01	0.13
	1.8	3.02	± 0.23	± 0.29	0.14	0.17	0.01	0.17
	1.9	2.44	± 0.20	± 0.21	0.11	0.17	0.02	0.05

TABLE A.IV: Results for $\langle (n_X^2 - \langle n_X^2 \rangle)^2 \rangle$ for all measured cuts on p_ℓ^*.

p_ℓ^* [GeV/c]	$\langle (n_X^2 - \langle n_X^2 \rangle)^2 \rangle$ [GeV^2]	$\sigma_{\rm stat.}$	$\sigma_{\rm stat.+sys.}$
0.8	1.20	0.34	0.57
0.9	1.15	0.25	0.28
1.0	1.08	0.16	0.21
1.1	0.78	0.12	0.17
1.2	0.71	0.10	0.16
1.3	0.60	0.08	0.14
1.4	0.56	0.07	0.13
1.5	0.52	0.06	0.14
1.6	0.39	0.05	0.08
1.7	0.27	0.05	0.08
1.8	0.21	0.05	0.09
1.9	0.16	0.06	0.09

TABLE A.V: Results for $\langle (n_X^2 - 1.35 \text{ GeV}^2)^2 \rangle$ for all measured cuts on p_ℓ^* .

p_ℓ^* [GeV/c]	$\langle (n_X^2 - 1.35 \text{ GeV}^2)^2 \rangle$ [GeV^2]	$\sigma_{\text{stat.}}$	$\sigma_{\text{stat.+sys.}}$
0.8	1.21	0.40	0.69
0.9	1.16	0.30	0.35
1.0	1.09	0.20	0.28
1.1	0.78	0.15	0.22
1.2	0.71	0.12	0.20
1.3	0.60	0.09	0.18
1.4	0.56	0.08	0.16
1.5	0.52	0.07	0.16
1.6	0.39	0.05	0.06
1.7	0.27	0.05	0.04
1.8	0.21	0.03	0.05
1.9	0.19	0.02	0.02

TABLE A.VI: Results for $\langle (n_X^2 - \langle n_X^2 \rangle)^3 \rangle$ for all measured cuts on p_ℓ^* .

p_ℓ^* [GeV/c]	$\langle (n_X^2 - \langle n_X^2 \rangle)^3 \rangle$ [GeV^3]	$\sigma_{\text{stat.}}$	$\sigma_{\text{stat.+sys.}}$
0.8	4.19	2.38	3.92
0.9	3.99	1.85	1.99
1.0	3.33	1.13	1.36
1.1	1.26	0.66	0.84
1.2	0.96	0.43	0.67
1.3	0.68	0.34	0.59
1.4	0.57	0.22	0.53
1.5	0.51	0.18	0.53
1.6	0.18	0.12	0.17
1.7	0.18	0.11	0.16
1.8	0.19	0.12	0.19
1.9	0.16	0.15	0.21

TABLE A.VII: Results for $\langle (n_X^2 - 1.35 \text{ GeV}^2)^3 \rangle$ for all measured cuts on p_ℓ^* .

p_ℓ^* [GeV/c]	$\langle (n_X^2 - 1.35 \text{ GeV}^2)^3 \rangle$ [GeV^3]	$\sigma_{\text{stat.}}$	$\sigma_{\text{stat.+sys.}}$
0.8	4.57	3.31	5.58
0.9	4.33	2.54	2.85
1.0	3.62	1.59	2.04
1.1	1.36	0.98	1.33
1.2	1.01	0.66	1.08
1.3	0.69	0.52	0.94
1.4	0.53	0.36	0.82
1.5	0.46	0.29	0.80
1.6	0.14	0.16	0.22
1.7	0.13	0.10	0.16
1.8	0.14	0.09	0.16
1.9	0.08	0.09	0.15